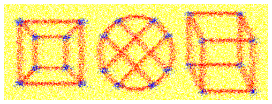
Journal of Graph Algorithms and Applications
http://jgaa.info/ vol. 18, no. 1, pp. 35–76 (2014)
DOI: 10.7155/jgaa.00314

Generalizing Geometric Graphs

Edith Brunel[1] *Andreas Gemsa*[1] *Marcus Krug*[1] *Ignaz Rutter*[1]
Dorothea Wagner[1]

[1]Faculty of Informatics, Karlsruhe Institute of Technology (KIT), Germany

Abstract

Network visualization is essential for understanding the data obtained from huge real-world networks such as flight-networks, the AS-network or social networks. Although we can compute layouts for these networks reasonably fast, even the most recent display media are not capable of displaying these layouts in an adequate way. Moreover, the human viewer may be overwhelmed by the displayed level of detail. The increasing amount of data therefore requires techniques aiming at a sensible reduction of the visual complexity of huge layouts.

We consider the problem of computing a generalization of a given layout reducing the complexity of the drawing to an amount that can be displayed without clutter and handled by a human viewer. We take a first step at formulating graph generalization within a mathematical model and we consider the resulting problems from an algorithmic point of view. We show that these problems are NP-hard in general, and provide efficient approximation algorithms as well as efficient and effective heuristics. We also showcase some sample generalizations.

Submitted:	Reviewed:	Revised:	Reviewed:	Revised:
March 2013	August 2013	October 2013	December 2013	January 2014
	Accepted:	Final:	Published:	
	January 2014	January 2014	January 2014	
	Article type:	Communicated by:		
	Regular paper	S. Kobourov		

A preliminary version of this paper has appeared as "Generalizing Geometric Graphs" in *Proceedings of the 19th International Symposium on Graph Drawing (GD'11)*, vol. 7034 of LNCS, pages 170–181. Springer, 2012.

E-mail addresses: edith@brunel-online.de (Edith Brunel) gemsa@kit.edu (Andreas Gemsa) krug.marcus@gmail.com (Marcus Krug) rutter@kit.edu (Ignaz Rutter) dorothea.wagner@kit.edu (Dorothea Wagner)

1 Introduction

As a natural consequence of the increasing amount of available data we are frequently facing large and even huge networks such as road and flight networks, the Internet and social networks with millions of vertices. Visualization of these networks is a key to assessing the inherent graph-based information via human inspection. There are several methods for computing layouts of huge graphs with millions of vertices within a few minutes [28, 31, 25].

But, how do we display such layouts? Modern HD displays feature roughly 2 Mio pixels and a standard A4 page allows roughly 8.7 Mio dots at a resolution of 300 pixels per inch. Although these numbers do sound adequate for large-scale graph visualization at first glance, both media are not at all suited for displaying huge graphs with millions of vertices. Even if we require only a minimal distance of 10 pixels or dots between the vertices of the graph, which yields a distance between vertices of roughly 3 millimeters on the screen and less than 1 millimeter on paper, then we can display only several thousand vertices, and not too many edges. If we additionally seek to display graph structure and keep visual clutter low, the number of vertices we can display degrades even further and may go down to less than a hundred for dense graphs.

Even worse, the human perception is not capable of extracting detailed information from huge layouts with millions of vertices. Since, by a simple counting argument, there are incompressible adjacency matrices [32], a graph with only 1 Mio vertices may encode incompressible information of up to 125 Gigabytes. This exceeds by a factor of 3.6 the average daily information consumption of an average American estimated at 34 (highly compressible) Gigabytes of information in the current report on American Consumers [6].

To get around these fundamental barriers in visualizing graphs, we propose to compute and display *generalizations of graphs* that appropriately reduce the amount of information that is displayed in a drawing such that the result can be properly perceived by the viewer and still contains the major parts of the original information. In particular, we seek to reduce the amount of incompressible detail information that the user is not capable of absorbing anyway due to cognitive limitations. We stress that a generalization of a graph with a fixed layout is again a (usually much smaller) graph together with a fixed layout that preserves both visual appearance and graph-theoretical properties of the original, such as density, connectivity, and planarity.

Our model is based on the fact that vertices have a fixed size and edges have a fixed width on the screen. *Visual clutter* refers to an agglomeration of overlapping visual features in a limited area that renders these features indistinguishable. Our goal is to either avoid or reduce visual clutter. We identify three types of clutter.

Vertex-Clutter occurs when two or more vertices are too close to each other. It may render the drawing unusable due to hidden edge information; see Fig. 1a.

Edge-Clutter occurs when too many edges cross a limited area. Even if ver-

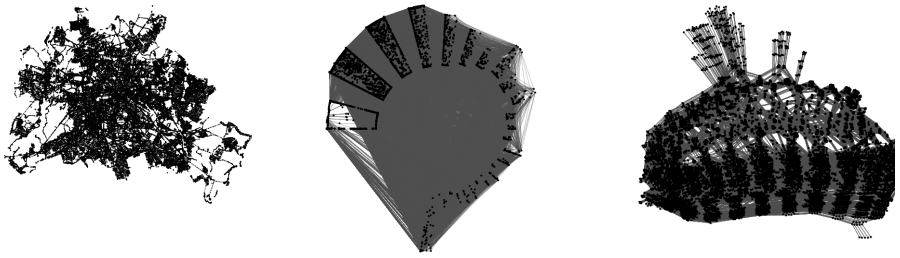

(a) Vertex-Clutter (b) Edge-Clutter (c) Vertex-Edge-Clutter

Figure 1: Illustration of the different types of visual clutter.

tices are far enough apart, edge clutter may lead to indistinguishable edge information; see Fig. 1b.

Vertex-Edge-Clutter occurs when a vertex is too close to an edge. In this case, we are unable to tell, whether the vertex is incident to the edge or not; see Fig. 1c.

The generalization should maintain the spirit of the drawing of the graph and preserve the prominent features while reducing the amount of detailed information to an amount that can be displayed without clutter and handled by a human viewer.

Related Work Known approaches to coping with the huge amount of data by allowing for some kind of abstraction can be categorized into *structural* and *geometric* methods. While structural methods create a new layout for the data, typically using a clustering of the graph, geometric methods are applied to a given layout maintaining the user's mental map [35].

Graph-theoretic clustering methods, which can be used to cluster the graph for visualization are discussed in [20]. Eades and Feng [17] describe a multilevel visualization method for clustered graphs with the aim of visualizing network-based data that has been clustered hierarchically at different levels of abstraction induced by the hierarchy of the clustering. A force-directed layout algorithm based on a hierarchical decomposition of the graph is given by Quigley and Eades [37]. This method allows for visualizing the graph at different levels of abstraction by computing a layout based on a hierarchical grouping of the vertices of the graph. Harel and Koren [27] present a multi-scale algorithm with the purpose of producing nice drawings on large and small scale, respectively. Different levels of abstraction of the graph are obtained by iteratively coarsening the graph. Other scalable force-directed drawing algorithms based on the multi-scale paradigm are given by Gajer and Kobourov [21], Gajer et al. [21] and Walshaw [42]. Multi-scale drawing methods are combined with fisheye views by Gansner et al. [22]. Their approach is to compute a layout of a graph whose level of detail deteriorates with increasing distance to the focal node

of the layout, that is, they provide a topological version of classical fisheye visualization techniques. Abello el al. [4] discuss graph sketches for very large graphs based on mapping clusters of the graph to certain regions of the screen. Their notion of a sketch is based on a hierarchical clustering of the graph and is mainly focused on exploring the graph via a detail-on-demand strategy without providing a good approximation of the graph's structure and geometry. Rafiei and Curial [38] study the generalization of graphs by sampling.

Classical fisheye visualizations [19, 40], on the other hand, can be directly applied to a given layout and apply a distortion to a given layout to emphasize the structure of the drawing in a certain area of interest. The resolution of the drawing deteriorates towards the boundary of the drawing and parts of the drawing in this area are usually densely cluttered. Abello et al. [3] study the visualization of large graphs with compound-fisheye views and treemaps, employing hierarchical clustering and a treemap representation of this clustering. Edge Bundling techniques [41, 29] aim at reducing the complexity of layouts by bundling similar edges.

Generalization differs from structural methods in that it takes as input a fixed layout of a graph, rather than creating one that may be particularly well-suited to displaying the graph at different levels of granularity. Just like geometric methods, generalization can thus be applied to any given layout. The geometric methods, however, usually preserve the graph structure completely and only modify the view on the given layout to display detail information in certain focus areas, often leading to substantial amounts of clutter outside. Generalization has received considerable attention in cartography [34]. Mackaness and Beard [33] highlight the potential of graph theory for map generalization. Saalfeld states the map generalization problem as a straight-line graph drawing problem [39] and formulates a number of challenges resulting from this perspective. Among others, he asks for a rigorous mathematical model for graph-based generalizations and provable guarantees. We are not aware of any work aiming at assessing this problem to its full extent.

Contribution and Outline We devise a framework that allows for computing generalizations by eliminating, or at least reducing, all types of clutter in an incremental way by modeling the elimination or reduction of each type of clutter as an optimization problem, which we analyze in terms of complexity. We show that these problems are NP-hard in general and we provide approximation algorithms as well as effective and efficient heuristics that can be applied to huge graphs within reasonable time.

A key to assessing the problem of computing a suitable generalization is to find an adequate measure of the quality or appropriateness of a generalization. It is essential to understand the geometric and combinatorial features resulting in the visual complexity of geometric graphs and how they affect human perception. The *geometric features* of the drawing include, among others, the distributions of points and edges as well as the distribution of crossings, the shapes of the faces of the arrangement, especially the outer face, as well as

symmetries and other peculiarities of the drawing. The *combinatorial features* include connectivity, structure and length of shortest paths as well as, for instance, planarity. Although we are far from fully understanding the impact of these features on the human perception, we try to incorporate a carefully selected set of these features into our model of a generalization. This constitutes a first step towards establishing a mathematical model for the problem of generalizing geometric graphs.

In Section 2, we consider the problem of reducing vertex-clutter. We discuss our model for the generalization of the vertex set and show NP-hardness of the corresponding optimization problem. We further show that the size of the generalized pointset can be approximated efficiently and we devise an efficient heuristic for further optimization. In Section 3, we study the reduction of edge-clutter. We show that it is in general NP-hard to find a sparse or short subset of the edges maintaining monotone tendencies. When the original graph is complete, however, or if we are not restricted to use edges of the original graph, we can efficiently compute a sparse graph approximately representing monotone tendencies of the edges. In Section 4, we model the problem of reducing vertex-edge clutter and we show how to compute a drawing that allows for unambiguously deciding whether an edge is incident to a vertex or not, thus effectively eliminating vertex-edge clutter. We present a brief experimental evaluation and showcase some sample generalizations in Section 5 and conclude with a short discussion as well as open problems in Section 6.

Preliminaries. A *geometric graph* is a pair $G = (P, E)$ such that $P \subseteq \mathbb{R}^2$ is a finite set of n points in the plane and E is a set of m straight-line segments with endpoints in P. Unless stated otherwise, graph refers to a geometric graph throughout this paper. Throughout the paper distance refers to the Euclidean metric. For $p \in P$ and a non-negative number $r \in \mathbb{R}_0^+$, we denote by $B(p, r)$ the disk with center p and radius r. We model the finite resolution of a screen by assuming that each entity of the drawing, namely points and edges, indeed occupies a small neighborhood around it. Clutter is avoided by ensuring that the corresponding generalizations adhere to spacing constraints that avoid or reduce overlaps of these regions appropriately.

A *generalization* of G is a pair (H, φ) where $H = (Q, F)$ is a geometric graph with $Q \subseteq P$ such that $\varphi\colon P \to Q$ maps vertices of G to vertices of H and F is a subset of edges resulting from a contraction of G according to φ. We also call the pair (H, φ) a *generalized graph*. Since the subgraph induced by $\varphi^{-1}(\{q\})$ is contracted into a single vertex, we call this subgraph the *cluster* of q, denoted by C_q. Given $Q \subseteq P$, we denote by $\nu\colon P \to Q$ the *Voronoi mapping*, which maps $p \in P$ to its closest neighbor in Q with respect to the Euclidean metric. We call the corresponding clusters *Voronoi clusters*. We especially focus on this mapping since it minimizes $\sum_{p \in P} d(p, \varphi(p))$ and, hence, seems to be a natural mapping.

2 Generalizing the Vertex Set without Vertex-Clutter

In this section we consider the problem of computing a generalization (H, φ) without vertex clutter for a geometric graph $G = (V, E)$, where $H = (Q, F)$. We focus on the case that φ is the Voronoi mapping assigning each vertex in P to its nearest neighbor in Q. In order to avoid vertex-clutter, we require a minimal distance $r \in \mathbb{R}_0^+$ between the vertices of a generalized geometric graph. We model this minimal distance by a function $\varrho\colon P \to \mathbb{R}_0^+$ that assigns to each point $p \in P$ a positive real number $\varrho(p) \geq r$. We will later propose variants for choosing ϱ, which at least allow to give approximate guarantess. For each vertex $p \in Q$ in the generalized graph we require that the disk $B(p, \varrho(p))$ does not contain any other point from Q. We call a pointset Q with this property a *ϱ-set of P*. Note that the empty set or a singleton subset of P is trivially a ϱ-set of P. Thus, this prerequisite must be balanced with additional quality measures such as the size of the ϱ-set, the clustering $\{\varphi^{-1}(\{p\}) \mid p \in P\}$ induced by φ and the distribution of the points in Q in order to avoid trivial solutions such as a single vertex. Clearly, it is desirable to maximize the size of a ϱ-set in order to retain as many vertices of the original graph as possible. That is, even in the presence of other optimization goals we may assume that the vertex set Q of the generalization constitutes an inclusion-maximal ϱ-set of the original point set P.

Choosing $\varrho \equiv r$ uniformly for all points $p \in P$ may have a severe effect on the distribution of the points when maximizing the size of a ϱ-set since the distances to the nearest neighbors in an inclusion-maximal ϱ-set tend to be uniformly distributed regardless of the original distribution. However, it may be more appropriate to approximate the distribution of the original pointset. In order to approximate this distribution by an inclusion-maximal ϱ-set we can choose ϱ as follows. Let p_0 be the point that maximizes the number of points in $B(p, r) \cap P$ over all $p \in P$ and let $k = |B(p_0, r) \cap P| - 1$ denote the number of points in this disk that are different from p_0. For each $p \in P$ let $d_k(p) \geq r$ denote p's distance to its k-nearest neighbor in P. Choosing $\varrho(p) = d_k(p) \geq r$ preserves the original distribution of the point set better. Although clearly the pointset is stil thinned out until the minimum distance between any two points is r, it additionally ensures a larger spacing and thus fewer points in sparser areas of the input. Taking an (inclusion-)maximal ϱ-set with respect to this function additionally ensures that areas are not sparsened more than necessary to achieve the required spacing. In this sense a maximal ϱ-set approximately preserves the distribution of the original pointset.

Since, in general, it is not clear which behavior is more appropriate, we introduce a parameter $\alpha \in [0, 1]$ to control it by setting $\varrho(p) := \max\{r, \alpha d_k(p)\}$. That is, the user can choose between retaining as many points in areas with low clutter as possible ($\alpha = 0$) and approximating the distribution of the pointset ($\alpha = 1$) as well as interpolations between the two extremes. Note that $\varrho = \varrho_{r,\alpha}$ depends on r and α. For reasons of brevity we omit the subscripts.

We consider two measures to assess the quality of a ϱ-set Q. While the size of Q is a measure of the amount of data that is retained, the quality of the clustering induced by φ is a measure for the amount of data that is lost due to the contraction of the vertices. There are several established ways of assessing the quality of clusterings, such as coverage, performance, conductance [20], and modularity [9]. Since the information contained in the inter-cluster edges is retained in the generalization, we concentrate on assessing the quality of the clusters based on the intra-cluster edges. We consider a measure similar to coverage, which we adapt to our purpose as follows. For each cluster C_q let n_q denote the number of vertices and m_q denote the number of edges in C_q, respectively. We define the *local coverage* of a cluster C_q by $\operatorname{lcov}(C_q) = 2m_q/(n_q(n_q-1))$. The intuition is that the local coverage corresponds to the amount of intra-cluster coherence that is explained by the intra-cluster edges. Hence, a natural goal is to maximize this quantity. The local coverage of the generalization is defined as $\operatorname{lcov}(H,\varphi) = \min_{q\in Q} \operatorname{lcov}(\varphi^{-1}(\{q\}))$.

We consider the following multi-objective optimization problem. Given a geometric graph $G = (P, E)$, a non-negative radius $r \in \mathbb{R}_0^+$ and $\alpha \in [0, 1]$ the Local Coverage Cluster Packing (LCCP) problem is to compute a ϱ-set $Q \subseteq P$ and a mapping $\varphi\colon P \to Q$ that maximizes both $|Q|$ and $\operatorname{lcov}(H,\varphi)$.

Problem Local Coverage Cluster Packing (LCCP)

Instance: Geometric graph $G = (P, E)$, $r \in \mathbb{R}_0^+$, $\alpha \in [0, 1]$

Solution: ϱ-set $Q \subseteq P$, mapping $\varphi\colon P \to Q$

Goal: maximize $\operatorname{lcov}(H,\varphi)$, maximize $|Q|$

First we show that several single-criteria optimization variants of this multi-criteria optimization problem are NP-hard. Then we show how to approximate the size of a ϱ-set efficiently and we devise an efficient heuristic for balancing the size of a ϱ-set with the quality of the induced local coverage.

2.1 Complexity

We note that the decision problem corresponding to LCCP is obviously in NP, since, for any choice of parameters r and α, we can guess a set $Q \subseteq P$ and a corresponding mapping $\varphi\colon P \to Q$ and then verify in polynomial time that Q is indeed a ϱ-set and that its local coverage and size exceed the target values defined by the decision problem. In the following we show that LCCP is in fact NP-hard (and thus NP-complete), even if we only seek to maximize either the size or the local coverage of the ϱ-set.

The problem of computing a ϱ-set of maximum size for $\alpha = 0$ can be reduced to the problem of computing a maximum independent set in the intersection graph of the disks with radius $r/2$ centered at the points in P. Clark et al. [13] prove that this problem is NP-hard in unit-disk graphs, even if the disk representation of the graph is given.

Theorem 1 *Maximizing the size of a ϱ-set is NP-hard for $\alpha = 0$.*

Next, we show that, even if we use the Voronoi mapping to define the induced clustering, then it is NP-hard to find a ϱ-set Q that (i) maximizes the local coverage of the induced clusters or (ii) maximizes the size of Q subject to a lower bound on the local coverage. In fact, we will show that it is even NP-complete to decide whether a graph admits a *perfect ϱ-set*, that is a ϱ-set with local coverage 1. Note that the local coverage of a cluster is 1 if and only if it forms a clique. Thus, a ϱ-set Q of a geometric graph G is perfect if and only if the graphs induced by the vertices in each of the Voronoi faces defined by Q are cliques. We will use the following lemma.

Lemma 1 *Let C be a clique of a geometric graph G, such that C has a vertex whose neighborhood is contained in C. Every perfect ρ-set of G contains a vertex of C.*

Proof: Assume for a contradiction that Q is a perfect ϱ-set and $Q \cap C = \emptyset$. Let $p \in C$ whose neighborhood is contained in C. It follows that p is in the cluster C_q of some vertex q of G with $q \notin C$. In particular p is not adjacent to q, and thus C_q does not form a clique. Hence $\text{lcov}(Q) \leq \text{lcov}(C_q) < 1$, contradicting the assumption that Q is perfect. □

We are now ready to present the NP-hardness result.

Theorem 2 *Maximizing $\text{lcov}(H, \nu)$ of a generalization (H, ν) is NP-hard for $\alpha = 0$.*

Proof: The proof is by reduction from the NP-hard problem Planar Monotone 3-sat [15]. Let $\mathcal{U} = \{x_1, \ldots, x_n\}$ be a set of boolean variables and let $\mathcal{C} = C_1 \wedge C_2 \cdots \wedge C_m$ be a 3-sat formula. Then $\mathcal{C}$ is called *monotone* if all clauses consist only of positive or only of negative literals. Let $\mathcal{G} = (\mathcal{U} \cup \mathcal{C}, \mathcal{E})$ be the bipartite graph, on the clauses and variables, where $\mathcal{E}$ contains the edge (x_i, C_j) if and only if the literal x_i or its negation is contained in C_j. A *monotone rectilinear representation* of a monotone 3-sat formula is a rectilinear drawing of $\mathcal{G}$ such that the following conditions are met, as illustrated in Figure 2.

(i) The variables and clauses are drawn as axis-aligned non-overlapping boxes of uniform height such that all variable boxes are positioned on the x-axis, clauses containing only positive literals are positioned above the x-axis, and clauses containing only negative literals are positioned below the x-axis.

(ii) The edges are drawn as vertical line segments connecting the corresponding boxes.

(iii) The drawing does not contain any crossings.

An instance of Planar Monotone 3-sat consists of a *monotone rectilinear representation* of a planar monotone 3-sat instance and we wish to decide,

whether the corresponding 3-SAT instance is satisfiable. Given a monotone rectilinear representation of a planar monotone 3-SAT formula we will construct a corresponding instance $I = (G = (P, E), \varrho)$ of problem LCCP such that I contains a perfect ϱ-set if and only if the 3-SAT formula is satisfiable. For reasons of simplicity our construction is based on a disconnected graph with collinear points, but the construction can be modified in a straightforward way to obtain similar results for connected graphs with vertices in general position. We return to this at the end of the proof. We choose $\varrho \equiv 1.25$ and we construct G from a set of *variable/literal gadgets*, *transmitter/bend gadgets* and *clause gadgets*, which we will describe subsequently.

Variable/Literal Gadget. We distinguish between *basic* and *extended* variable and literal gadgets, respectively. The basic variable gadgets incorporate the functionality needed to correctly represent the variables. These gadgets can be extended to transmit their state along the transmitters. Each basic variable gadget consists of three vertically aligned cliques of size three, four, and three, respectively, as illustrated in Figure 3. Each clique consists of vertically aligned points at distance 1, and the cliques are separated by a vertical gap of 0.5.

Due to Lemma 1 a perfect ϱ-set of G must contain at least one vertex in each of the cliques. Note that we cannot choose two vertically consecutive vertices in any of the cliques, since they do not constitute a ϱ-set. For two consecutive cliques C and C' we define their bisector as the bisector between their closest points. Let p and q be vertices of C and C' in a perfect ϱ-set. We claim that it follows from the chosen vertical positions of the points that p and q must be positioned symmetrically with respect to the bisector of C and C'. Assume they are not positioned symmetrically, as for example in Figure 3d. Then the bisector of these points intersects the edges of one of the cliques, which implies that one of the clusters contains vertices from both C and C'. The corresponding cluster then has local coverage strictly less than 1. Furthermore, even though they are symmetric to the bisector of C and C', we cannot choose the two vertices closest to the gap for p and q, since they do not constitute a ϱ-set. Hence, there are only two valid ϱ-sets of the basic variable gadget, corresponding to the true and false state of the corresponding variable, as illustrated in Figure 3b and 3c, respectively. To be able to transmit the states of variables, we need

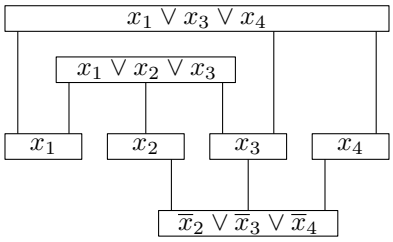

Figure 2: Monotone rectilinear representation of the 3-SAT formula $(x_1 \vee x_2 \vee x_3) \wedge (x_1 \vee x_3 \vee x_4) \wedge (\overline{x}_2 \vee \overline{x}_3 \vee \overline{x}_4)$.

to connect them to transmitter gadgets. To make this possible, we extend the variable gadgets by substituting the cliques of size 3 where we want to copy the state by a clique of size 4; see the places where variable states are copied in Figure 6. In this way, the situation of two 4-cliques meeting is the same both inside the variable gadget and at the meeting point of the variable gadget and the transmitter.

The literal gadgets are composed of basic and extended variable gadgets that are horizontally aligned. The horizontal gap between the gadgets is variable and can be chosen to be 1 or 1.5, as illustrated in Figure 4. The different possible spacings allow us to slightly stretch the construction in order to realize all distances correctly. This is necessary since the transmitter and clause gadgets are quite rigid.

Note that, due to the monotonicity of the formula, it is sufficient that our variables pass their state to the top and the negation of that state to the bottom. In particular, we do not need a gadget for producing the negation of a given state.

Transmitter/Bend Gadget. Similar to the variable gadget, the transmitter gadgets consist of two vertically aligned cliques of size 4 with consecutive vertices at distance 1 such that the cliques are separated by a gap of 0.5. When stacked upon the extended variable gadgets with a vertical gap of 0.5 the transmitter gadgets can be in one of two valid states corresponding to the assignment of the variable. The bend gadgets consist of one vertical and one horizontal transmitter gadget as illustrated in Figure 5. The positions are such that the coordinates of the two closest vertices of the two transmitter gadgets differ by 0.5 in both the x- and y-coordinate.

Figure 5c illustrates that the state cannot change at the transition between the horizontal and the vertical transmitter segment. Such a change would result in local coverage strictly smaller than 1.

Clause Gadget. Finally, the clause gadget is constructed as illustrated in Figure 5. It consists of three small gadgets, called *connectors*, each consisting of two cliques of size three and four, respectively, that are arranged in a T-shaped fashion. The connectors are constructed exactly as the topmost two cliques of the basic variable gadget. The functionality of the clause is realized by a small triangle (which is a clique of size 3) arranged in the middle of the T-shaped figure. The vertices of the triangle are positioned as follows. The left vertex is positioned on the same horizonal line as the left connector and has distance slightly larger than 1, say 1.1, from the rightmost vertex of the left connector. The right vertex is positioned symmetrically, at distance 1.1 to the left of the leftmost vertex of the right connector. The bottom vertex of the triangle is positioned vertically above the lower connector at distance 1.1 from its topmost vertex. If all literals corresponding to the clause are false, then each of the triangle's vertices is contained in the ϱ-disk of one of the vertices contained in the corresponding ϱ-set. Hence, none of the vertices of the triangle may be contained in the ϱ-set and, thus, the vertices of the triangle are mapped to a neighboring point resulting in local coverage strictly less than 1. This is

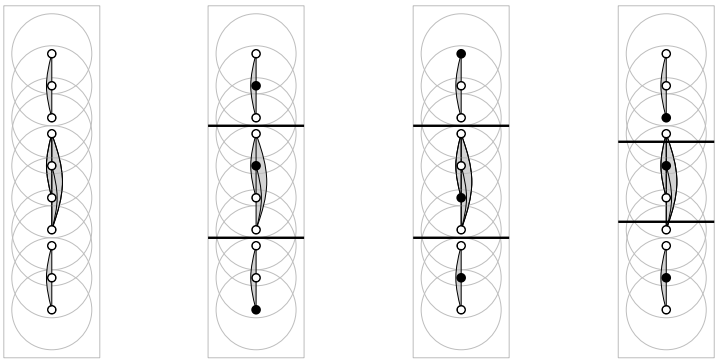

(a) Basic variable (b) True (c) False (d) Illegal

Figure 3: Variable gadget

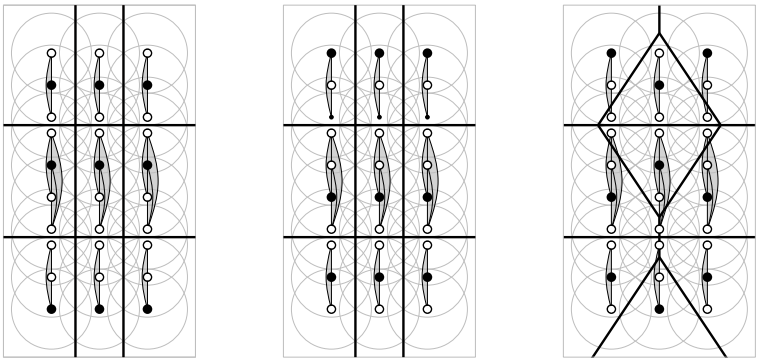

(a) True (b) False (c) Illegal

Figure 4: Literal gadget

illustrated in Figure 5e. If, on the other hand, at least one of the variables is in a true state, then one of the triangle's vertices can be included in the ϱ-set. The positions of the vertices of the triangle are chosen in such a way that the bisector between any of these vertices and the closest vertex corresponding to a true assignment does not intersect any of the cliques of the clause. As illustrated in Figure 5d, this leads to a Voronoi diagram that does not intersect the edges of G, resulting in a perfect ϱ-set.

Clearly, a satisfying assignment of the 3-SAT formula can be transformed into a perfect ϱ-set of G. Conversely, assume that we are given a perfect ϱ-set of G. As argued, the variable gadgets can be in one of two states, as illustrated in Figure 3. This state is likewise represented in the adjacent transmitters and will thus be transmitted without error to the clauses. Since the ϱ-set is perfect, one of the central triangle's vertices of each clause gadget must be in the set. Hence,

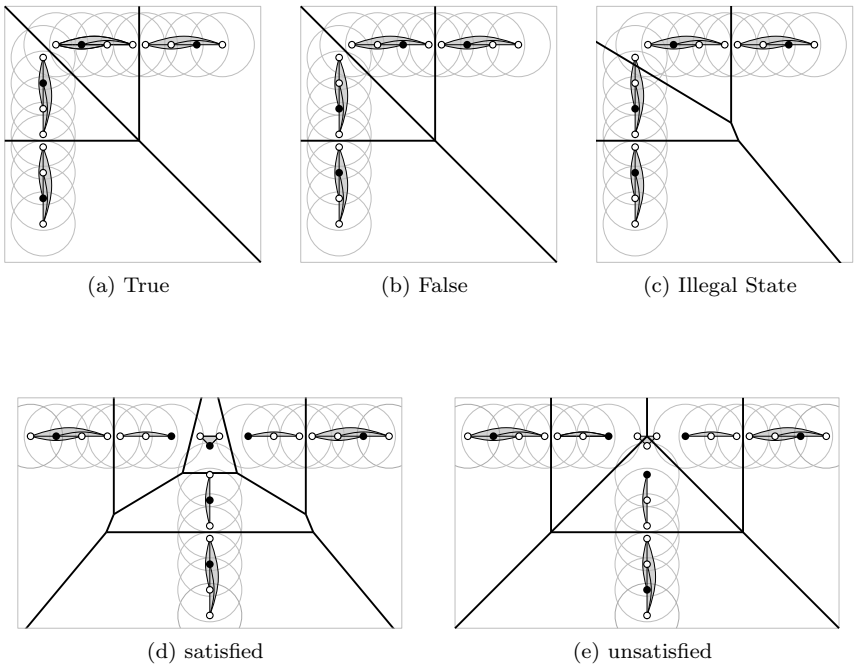

(a) True (b) False (c) Illegal State

(d) satisfied (e) unsatisfied

Figure 5: (5a)–(5c) Bend gadget, (5d)–(5e) Clause gadget.

at least one of the adjacent transmitters must be in a true state, corresponding to the assignment of one of the literals. Hence the states of the variables as in Figure 3 correspond to a satisfying assignment of the 3-SAT formula. A sample reduction is illustrated in Figure 6.

We now argue that, given a monotone rectilinear representation of a formula φ where the variable-clause graph is embedded on a grid can be converted into the described graph G in polynomial time. By suitably blowing up the grid, we create sufficient space to position the variable and clause gadgets. Note that a polynomial factor suffices, since each variable occurs only polynomially often. Moreover, for each clause, we may have to additionally stretch some variables to ensure that the corresponding transmitters start at x-coordinates that allow them to meet exactly as specified in the construction of the clause gadget. This is achieved by exploiting the two possible spacing values between variable gadgets of the same literal. Since the amount of space we have to bridge in this way is bounded by the width of two 4-cliques in the horizontal part of the left/right transmitters, a constant blowup per clause is sufficient. Thus, the overall construction has only polynomial size, and it can be carried out in polynomial time. This completes the proof. We add two more remarks.

Since the reduction is based on deciding whether the given graph contains a perfect ϱ-set whose size is equal to the number of cliques in G it yields that

both the maximization of local coverage as well as the maximization of the size of the ϱ-set with given minimum local coverage are NP-hard.

Obviously slightly perturbing the points does not change the combinatorial structure of the problem, and hence the hardness proof also holds for points in general position. Moreover, a connected instance can be obtained as follows. After the reduction, add an additional small triangle (which is a clique of size 3) far away from the remaining points and connect one of its vertices to one vertex of each other connected component of G. Note that this preserves the property that each of the cliques used in the construction of G contains a vertex whose neighborhood is contained in that clique, and thus Lemma 1 still applies. By placing the new vertices sufficiently far away, it can be ensured that they do not interact with the remaining ϱ-set of G. Thus, the NP-hardness result also holds for connected input graphs. □

2.2 Approximating the Maximum Size of a Generalization

Although it is unlikely that we can efficiently compute a ϱ-set with maximum size, we show that we can approximate the size of a maximum ϱ-set if the points are in general position. The approximation ratio depends on the maximum number k of points contained in any ϱ-ball of a point of the input, excluding the center point itself. Clearly, if $k = 0$, then the pointset itself is a ϱ-set, which is of course optimal. Thus, the following approximation result only makes sense for $k \geq 1$.

Theorem 3 *Let G be a geometric graph whose points are in general position and let $r \in \mathbb{R}_0^+$ and $\alpha \in [0, 1]$ be given. In $O(kn + n \log n)$ time we can compute a generalization $\mathcal{H}$ of G that approximates the maximum number of vertices of a generalization by a factor of $(5k+2)/3$, where $k = \max_{p \in P} |B(p, \varrho(p)) \cap P| - 1$ is assumed to be at least 1.*

Proof: Let H be the directed graph on the points of G such that pq is a (directed) edge if and only if $q \in B(p, \varrho(p))$. We prove that the graph H contains an independent set of size s if and only if G contains a ϱ-set of this size as follows. Each independent set in H corresponds to a ϱ-set in G, since each point in H is connected to all points that are closer than $\varrho(p)$ and it is connected to all points q such that p is in the $\varrho(q)$-disk around q. On the other hand, each ϱ-set in G induces an independent set due to this construction.

Note that H is a subgraph of the k-nearest-neighbor graph, whose maximum degree is bounded by $5k$ if the points are in general position [8]. Hence, by a result due to Halldórsson and Radhakrishnan [26], we can approximate the maximum size of an independent set by a factor of $(5k + 2)/3$. The algorithm greedily chooses the minimum-degree vertex in each step and can be implemented to run in time $O(kn)$, given the graph H.

In order to compute H, we first compute the k-nearest-neighbor graph in $O(kn + n \log n)$ time, using a well-separated pair decomposition [10]. Then we filter out the edges that are not contained in H in $O(kn)$ time. Hence, the total running time is $O(kn + n \log n)$. □

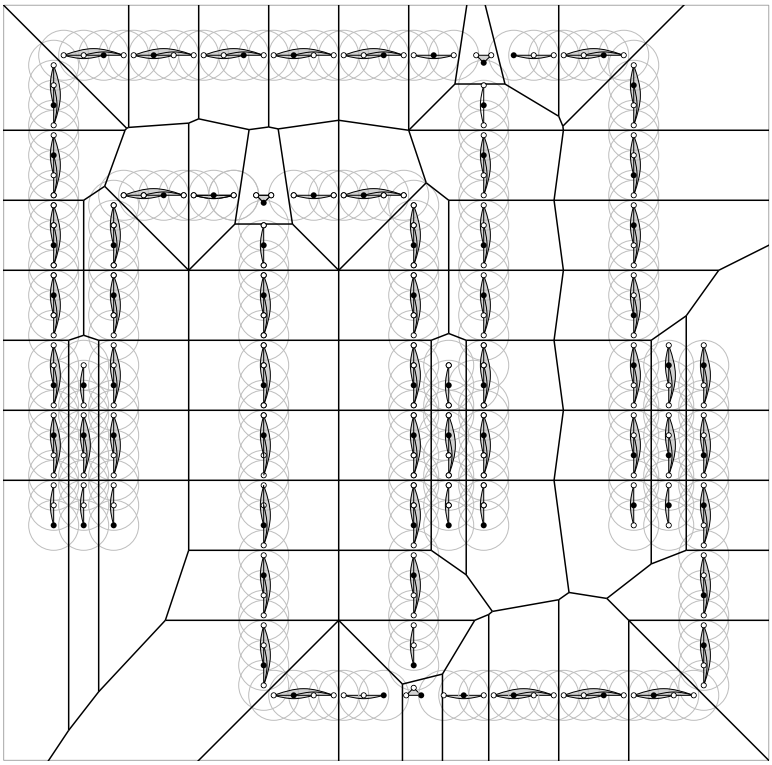

Figure 6: Sample reduction of the 3-SAT formula $(x_1 \vee x_2 \vee x_3) \wedge (x_1 \vee x_3 \vee x_4) \wedge (\overline{x}_2 \vee \overline{x}_3 \vee \overline{x}_4)$. The black points constitute a perfect ϱ-set corresponding to the assignment $x_1 = \text{true}, x_2 = \text{true}, x_3 = \text{true}, x_4 = \text{false}$.

Based on this approximation, we heuristically compute a ϱ-set Q balancing both the size of Q and the local coverage of the Voronoi clustering induced by Q as follows. For $p \in P$ let $\widetilde{m}(p)$ denote the number of edges whose endpoints are both contained in $B(p, \varrho(p)/2)$ and let $\widetilde{n}(p)$ denote the number of points in $B(p, \varrho(p))$. We can use these values to compute an estimate of the local coverage as summarized in the following lemma.

Lemma 2 *Let Q be an inclusion-maximal ϱ-set and let $\alpha = 0$. Further, let $H = (Q, F)$ be the generalization obtained from $G = (P, E)$ by the Voronoi mapping ν. Then the value*

$$\min_{q \in Q} \left\{ \frac{2\widetilde{m}(q)}{\widetilde{n}(q)(\widetilde{n}(q) - 1)} \right\}$$

is a lower bound for $\mathrm{lcov}(H, \nu)$.

Proof: For $\alpha = 0$ we have $\varrho \equiv r$. Whenever p is chosen as a cluster center in Q, the points in $B(p, r/2)$ are closer to p than to any other point in Q since the closest point to p in Q has distance to p at least r. Hence, the edges in $B(p, r/2)$ are intra-cluster edges of C_p. On the other hand, the number of points in each of the clusters is bounded by $\widetilde{n}(p)$ whenever $\alpha = 0$ and Q is an inclusion-maximal ϱ-set. To see this, consider any vertex q that is not contained in $B(p, r)$, but is closer to p than to any other cluster center. Then q is contained in none of the disks centered in the cluster centers and, thus, q must be a cluster center itself, since Q is inclusion-maximal. Hence, the claim holds. □

Based on Lemma 2 we propose a heuristic, called Greedy Weight Heuristic, that operates as follows. First we compute an estimate of $2\widetilde{m}(q)/(\widetilde{n}(q)(\widetilde{n}(q)-1))$ for each $p \in P$. Subsequently, we sort the points according to these estimates in $O(n \log n)$ time and iteratively consider the points in this order. If the current vertex is not covered by the ϱ-disk of a previous vertex, then it is chosen for the ϱ-set, otherwise it is discarded.

Note that computing $\widetilde{m}(p)$ and $\widetilde{n}(p)$ exactly would require a circular range counting query. To get away with simpler data structures, we estimate these numbers by counting the number of vertices and edges in the bounding boxes of the disks $B(p, \varrho(p)/2)$, for which simpler data structures are known. To count the number of edges, we use a 4-dimensional range searching query on a data structure containing tuples of points corresponding to edges in E with query time $O(\log^3 m)$ [11]. We use the 2-dimensional counterpart to locate points. Further, we use a data structure for dynamic nearest neighbor queries with $O(\log^2 n)$ query time [5], into which we insert the selected points to decide whether the current point is covered by a previously selected point. The total running time is $O((n + m) \log^3 m + n \log^2 n)$.

3 Minimizing Edge-Clutter

In order to reduce the clutter resulting from an excess of edges in certain areas we must filter out some of the edges without destroying the visual appearance

of the graph. The total length of the edges seems to be a good measure for the clutteredness of the graph since it is proportional to the ink used for the drawing. While a minimum spanning tree will minimize this quantity, it is unlikely to preserve the visual appearance of the graph. We therefore require that monotone tendencies of the edges are preserved in order to best maintain the mental map of the adjacencies between vertices of the graph. This also motivated from a recent work by Huang et al. [30], whose controlled user experiments seem to suggest that geodesic paths are more likely to be explored when reading a graph drawing.

Let ℓ be a line in the plane and let $S = (p_1, \ldots, p_k)$ be a sequence of points. We say that S is *ℓ-monotone* if and only if the order of the orthogonal projections of $p_1, \ldots, p_k$ onto ℓ is the same as the order of the points in S. Let $G = (P, E)$ be a geometric graph and let (H, φ) be a generalization of G such that $H = (P, F)$, i.e., $F \subseteq E$. We say that H is a *monotone generalization of* G if for every edge $e \in E$ with endpoints p and q there is a p-q-path π_e in H such that π_e is ℓ_e-monotone, where ℓ_e is the line defined by the endpoints of e. Given $G = (P, E)$, the problem Shortest Geodesic Subgraph (SGS) asks for a monotone generalization H of G minimizing the total length of H.

Problem Shortest Geodesic Subgraph (SGS)

Instance: Geometric graph $G = (P, E)$

Solution: Monotone generalization $H = (P, F)$ of G

Goal: minimize total length of H

First, we show that Shortest Geodesic Subgraph is NP-hard.

Theorem 4 Shortest Geodesic Subgraph *is NP-hard.*

Proof: We reduce from Monotone 3-sat, a variant of 3-sat where each clause contains either only positive or only negative literals. Monotone 3-sat is NP-complete [23]. Let φ be an instance of Monotone 3-sat with variables $x_1, \ldots, x_n$ and clauses $C_1, \ldots, C_m$. We construct the following instance G_φ of Shortest Geodesic Subgraph. For each variable x we create a kite consisting of vertices ℓ, r, t and b as shown in Figure 7a. Note that the angles at b, ℓ and r are strictly less than $90°$, and the angle at t is strictly larger than $90°$. The two edges incident to the top vertex t are called *top edges*, the edges $b\ell$ and br are called the left and right *side edges*, respectively. We place the kites corresponding to all variables of φ so that their bottom vertices are equally spaced on the x-axis, their top vertices are also equally spaced on a horizontal line above the x-axis and the kites are disjoint. Denote by s_ℓ and s_r the slopes of the left and right side edges of a kite, respectively. Let R^+ be the region below the x-axis and to the right of the line through the bottom point of the rightmost kite with slope $-1/s_r$ (i.e., it is perpendicular to the right sides of the kites). Further, we denote by L^+ the region that is above the horizontal line defined by the topmost points of the kites and to the left of the line with

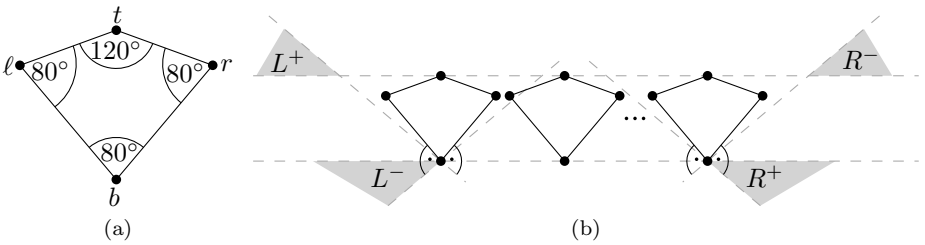

Figure 7: Overview of the reduction from 3-SAT to SHORTEST GEODESIC SUBGRAPH. A kite with bottom vertex b, top point t and left and right points ℓ and r (a), and the arrangement of the kites in the reduction with the corresponding regions for clause vertices (b).

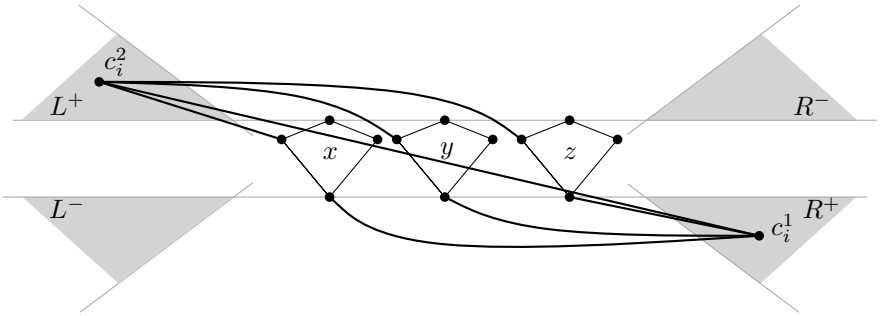

Figure 8: Construction for clause $C_i = x \vee y \vee z$

slope $-1/s_r$ through the bottom vertex of the leftmost kite. We define R^- and L^- analogously, with s_r replaced by s_ℓ.

It follows immediately from the construction that a path that is monotone with respect to a line defined by a point in R^+ and a point in L^+ may not contain any right edge of a kite as this would imply a turn of more than 90°, which is not monotone. Analogously, monotone paths from L^- to R^- may not contain left edges of kites. In our reduction the kites will play the role of variables, and edges from R^+ to L^+ (from L^- to R^-) will play the role of clauses with only positive (only negative) literals.

For each clause C_i consisting of only positive literals, we add a *clause vertex* c_i^1 into R^+ and a clause vertex c_i^2 in L^+. We add *connector edges* that connect c_i^1 to the bottom vertices of all kites that correspond to variables that occur in C_i and that connect c_i^2 to all the left points of kites that correspond to variables that occur in C_i; see Figure 8. Finally, we add the *clause edge* $c_i^1 c_i^2$. We treat the clauses consisting of only negative literals analogously, except that we place the new vertices in L^- and R^-, respectively, and we connect the new vertices in R^- to the right kite points instead of to the left.

This completes our construction, and we claim that an optimal solution of this instance allows us to decide whether the initial formula φ was satisfiable.

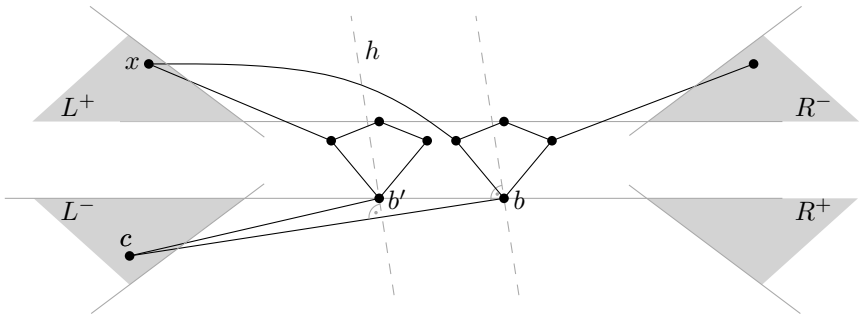

Figure 9: Illustration for the proof of the first claim. There is no monotone path in G_φ replacing the edge cb since every path avoiding this edge first visits a bottom vertex b' of a kite before it visits a point $x \in L^+$ whose orthogonal projection onto the line defined by c and b is to the left of the projection of b'.

We will make this more precise in the following. A subset of edges of G_φ is called *tight* if it contains both top edges of each kite, all connector edges, and exactly one of the two side edges of each kite. We now claim the following.

Claim 1 *Any feasible solution contains a tight edge set.*

Proof of claim. First, note that the top vertex of each kite is incident to only two edges, hence at least one of them must be in any feasible solution. However, the left edge is not monotone in the direction of the right edge and vice versa. Hence, a feasible solution necessarily contains both of them.

Next, we show that all edges from clause vertices in L^- or R^+ to bottom vertices of kites must be contained in every solution. Let c be a vertex in L^- (the case where c is in R^+ is symmetric) and let b be a bottom vertex of a kite that is adjacent to c. We now consider the paths from c to b that avoid the edge cb in our graph. Since G contains no edge connecting two vertices of different kites, any path from c to b that avoids cb must contain at least one vertex $x \neq c$ that is in one of the four regions L^+, L^-, R^-, and R^+. Note that, by construction of the region L^-, the line orthogonal to cb is at least as steep as the left side of any kite, and hence the points in R^- and in R^+ lie to the right of the line that is orthogonal to cb through b, and thus are not part of any monotone connection from c to b as illustrated in Figure 9. Now assume that x is in L^+ or L^-, and denote by b' the first vertex after c on a cb-path that avoids the edge cb. Note that necessarily b' is left of b, as the path would not be monotone otherwise. The regions L^+ and L^- lie to the left of the line h that is orthogonal to cb through b'. Therefore both the edge cb' and the subpath from x to b must cross this line, and hence project to the same point on the line segment from c to b. This shows that the path is not monotone, and hence cb must be contained in any feasible solution.

Next, consider a vertex c in L^+ and a corresponding edge $c\ell$ to the left vertex of a kite (again the case c in R^- and edge cr where r is the right vertex of a kite

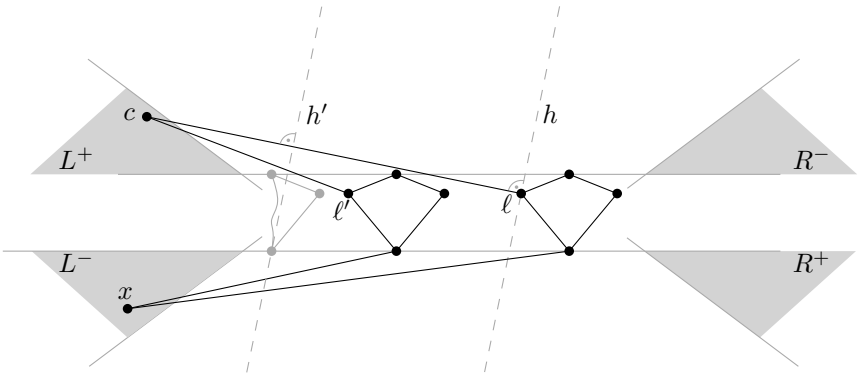

Figure 10: Illustration for the proof of the first claim. There is no monotone path in G_φ replacing the edge $c\ell$ since such a path would have to visit a vertex in one of the four regions L^-, L^+, R^-, R^+. By considering the lines h and h' this leads to a contradiction.

is symmetric); see Figure 10 for an illustration. As before, every path from c to ℓ avoiding $c\ell$ must contain a vertex $x \neq c$ belonging to one of the four regions. Again, the regions R^- and R^+ are to the right of the line hx orthogonal to $c\ell$ through ℓ, and can thus not be contained in a monotone $c\ell$-path. Hence, we can assume that x is in L^+ or L^-. Let ℓ' be the first vertex after c on a $c\ell$-path that avoids the edge $c\ell$. If x is in L^-, consider the line h' orthogonal to $c\ell$ through the bottom vertex of the leftmost skite. By construction this line is at least as steep as the right side of a kite, and hence the region L^- is to its left. Since any path from c to x must contain a bottom vertex b of a kite, both the subpath from c to x and the subpath from x to b must cross this line, and thus project to the same point on the edge $c\ell$. Hence the path would not be monotone and we can assume that x is in L^+. Considering the line orthogonal to $c\ell$ through the left point of the leftmost kite as above rules out the existence of such a monotone path.

It remains to show that at least one side edge of each kite must be in any feasible solution. Let b be the bottom vertex of a kite K with left point ℓ, right point r and top point t. We show that G does not contain a monotone $b\ell$-path that avoids both $b\ell$ and br. First observe that all bottom vertices of kites to the right of K project before b on the line through b and ℓ, directed from b to ℓ, and hence cannot be contained in a monotone $b\ell$-path. Similarly, all non-bottom vertices of kites to the left of K project behind ℓ on this line, and hence are also not contained in monotone $b\ell$-paths. The points in R^+ and all points in L^+ can be ruled out similarly. Since a monotone $b\ell$-path needs to contain an edge that connects a vertex whose y-coordinate is at most the y-coordinate of b to a vertex whose y-coordinate is at least the y-coordinate of ℓ, and we cannot use any edge of a kite, the only option is that it uses an edge from a vertex x in L^- to a vertex x' in R^- as illustrated in Figure 11. However, the line orthogonal to

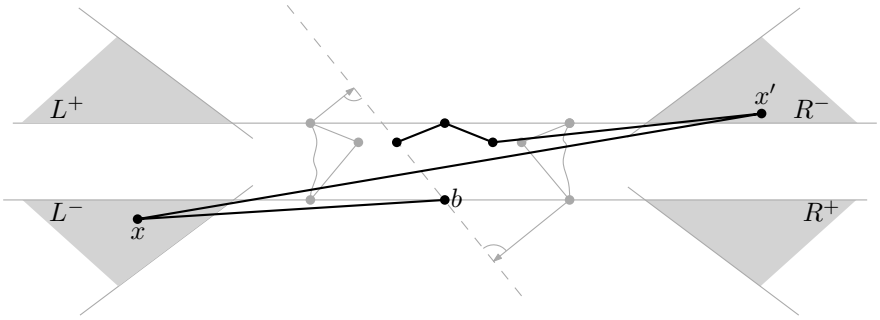

Figure 11: Illustration for the proof of the first claim. In each of the kites at least one of the side edges must be present. Otherwise, any replacing path for $b\ell$ must use an edge xx' that is not monotone with respect to $b\ell$.

such an edge is steeper than the edge $b\ell$, and hence xx' is not monotone with respect to $b\ell$. This completes the proof of the claim. ∎

Note that the size, as well as the total length, is the same for all tight edge sets, and hence this size forms a lower bound for the size of a geodesic subgraph. We claim that this bound can be met if and only if φ is satisfiable.

Claim 2 *There exists a tight set that is feasible if and only if φ is satisfiable.*

Proof of claim. Note that a tight set is completely specified by giving for each kite the information whether its left or right edge is contained in the set.

Assume that φ is satisfiable and take a satisfying assignment. We construct a tight set F by taking the left side of a kite if and only if the corresponding variable has the value *true* in the assignment. We now argue that the corresponding set is feasible. The only edges for which we have to check the existence of a monotone replacement path are the clause edges. Let $c_i^1c_i^2$ be a clause edge with c_i^1 in R^+ and c_i^2 in L^+. The edge $c_i^1c_i^2$ by construction corresponds to a clause C_i with only positive literals. Let x_j be a satisfied literal (and thus a satisfied variable) in C_i, and let K_j denote the corresponding kite with bottom vertex b and left point ℓ. By construction F contains the edges $c_i^1b, b\ell$ and ℓc_i^2, which together form a monotone $c_i^1c_i^2$-path. The argument for a clause edge $c_i^1c_i^2$ with c_i^1 in L^- and c_i^2 in R^-, which corresponds to a clause with only negative literals, is analogous. This proves that the tight set F is feasible.

Conversely, assume that F is a feasible tight set. We construct a truth assignment by setting a variable to true if and only if the left edge of the corresponding kite is in F. Now consider a clause C_i containing the variables x_u, x_v and x_w as positive literals (the case of only negative literals is symmetric). If C_i is not satisfied by our assignment, then F contains none of the left edges of the three kites corresponding to x_u, x_v and x_w. However, by definition the edge set must contain a monotone $c_i^1c_i^2$-path. Such a path may not use any right edge of any kite as this would not be monotone. Hence it necessarily contains

a left edge of some kite since F does not contain any of the clause edges. This implies that any monotone path must first visit the bottom vertex of one of the kites corresponding to x_u, x_v, x_w, then pass on to a vertex $x \neq c_i^1$ in L^- or R^+ and from there to the bottom vertex of another kite. By construction all points in R^+ lie to the right of the line that is orthogonal to $c_i^1 c_i^2$ through the bottom vertex of the rightmost kite. This excludes the case that x is in R^+. Similarly, the line orthogonal to $c_i^1 c_i^2$ through the bottom vertex of the leftmost kite separates the points in R^- from the bottom vertices of all kites. Hence the edges from x to its two incident bottom vertices both cross this line and hence the path is not monotone. This is a contradiction, and hence F must contain the left edge of at least one of the kites corresponding to x_u, x_v and x_w, thus implying that C_i is satisfied. This proves the claim. ∎

Note that the length L is the same for all tight edge sets. The first claim shows that any geodesic subgraph has length at least L. And thus, the second claim implies that φ is satisfiable if and only if G_φ admits a geodesic subgraph of length at most L. Since the construction can easily be performed in polynomial time this concludes the proof. □

As we have seen, the restriction to edges from the input graph makes it difficult to construct short monotone subgraphs. One possibility is thus to drop this constraint and to allow arbitrary edges. Additionally, we would like to control the distance of the monotone path π_e and the edge e it is approximating in terms of monotonicity. This is motivated by the observation that the shortest monotone generalization of a clique, whose vertices are arranged equidistantly on a circle, is given by the convex hull of the pointset.

Observation 1 *The shortest monotone generalization of a clique on $n \geq 5$ vertices that are arranged equidistantly on a circle is the convex hull of the pointset.*

Proof: Clearly, the convex hull forms a monotone generalization. We prove that it has minimum length.

Assume that n is odd and consider a monotone generalization of the clique. Let p and q be two consecutive vertices on the convex hull for which the segment is not part of the monotone generalization. It follows that the edge pq must be represented by the path psq, where s is the unique (since n is odd) vertex opposite to pq. We call the edges ps and sq the alternative edges for pq. Note that both ps and sq are strictly longer than pq. Moreover, each edge can be an alternative edge for at most two distinct segments formed by consecutive vertices. It follows that removing all inner edges and completing the convex hull shortens the network.

For n even similar arguments apply, except that there are three possible alternatives for each segment, some of whose edges can be shared by two but not more segments. □

Given a line segment s with length ℓ_s and a point p with distance d_p from s we call the ratio d_p/ℓ_s the *drift of p from s*. The *drift of a path π_e* with endpoints pq

is defined as the maximum drift of any point on π_e from the segment pq. Given a geometric graph $G = (P, E)$ and a non-negative real number $\delta \in \mathbb{R}_0^+$ the Sparse Geodesic Network (SGN) problem asks for a geometric graph $H = (P, F)$ with minimum total length such that for each edge e in E there is an ℓ_e-monotone path π_e in H with drift at most δ, where ℓ_e denotes the line defined by the endpoints of e.

Problem Sparse Geodesic Network (SGN)

Instance: Geometric graph $G = (P, E)$, $\delta \in \mathbb{R}_0^+$

Solution: Geometric graph $H = (P, F)$ such that H contains an ℓ_e-monotone path for each edge $e \in E$ whose vertices are at distance at most $\delta \cdot |e|$ from the straight line e

Goal: minimize the total length of the edges in F

We show the following.

Lemma 3 *Given a (complete) geometric graph $G = (P, E)$, the Delaunay graph contains for each edge $e \in E$ an ℓ_e-monotone path π_e with drift at most $1/2$.*

Proof: Let $p, q \in P$. Without loss of generality we assume that p and q are on the x-axis such that $x(p) < x(q)$. According to Dobkin et al. [16] we can construct an x-monotone path in the Delaunay graph $\mathcal{D}(P)$ of P as follows. Let $\mathcal{V}(P)$ denote the Voronoi diagram of P and let $p_1, \ldots, p_k$ be the ordered points corresponding to the Voronoi cells that are traversed when following the line from p to q. Then the path $p, p_1, \ldots, p_k, q$ is an x-monotone path in the Delaunay graph. Further, all points p_i are contained within the disk with radius $d(p, q)/2$ centered in the midpoint of the segment pq. Hence, the drift is at most $1/2$. □

Although the Delaunay graph seems to be well suited to represent monotone tendencies, this result also shows the limitations of allowing arbitrary edges. In the following we therefore focus on subgraphs of the original graph and describe a greedy heuristic for computing a monotone generalization with bounded drift δ and short total length, which we call Monotone Drift Heuristic. Given a geometric graph $G = (P, E)$ and a maximal drift δ we sort the edges of G with respect to increasing length in $O(m \log m)$ time. Then we consider the edges $e_1, \ldots, e_m$ in this order and iteratively construct a sequence of graphs $H_0, H_1, \ldots, H_m$, where $H_0 = (P, \emptyset)$. We insert the edge e_i into H_{i-1} whenever there is no ℓ_{e_i}-monotone path with drift at most δ in H_{i-1}. This can be tested by performing a modified depth-first search exploring only monotone subpaths in $O(n + m)$ time. Hence, the total running time of this approach is $O(nm + m^2)$.

4 Vertex-Edge-Clutter

Vertex-edge-clutter is the most complicated type of clutter since it involves both vertices and edges and the selection of these features cannot be handled independently as in the previous sections. On the other hand, this type of clutter may be considered as the least annoying type of clutter for the following reason. Vertex-edge clutter is caused by edges that are close to a vertex. This may make it difficult to determine correct incidences. There are two ways in which vertex-edge clutter can lead to a misinterpretation of a drawing: (a) an edge crossing a vertex might be interpreted as two edges incident to that vertex and (b) two segments incident to a vertex that form an angle close to 180° might be interpreted as one edge that is not incident to the vertex. However, the human perception is rather good at determining whether a line passes a disk through the center or not. For instance, it is easy to see that the leftmost line in Figure 12 is not incident to the vertex although it crosses the vertex, thus impeding misinterpretation (a). Additionally, the human perception is also good at determining whether a line has a bend or not, which is illustrated in Figure 12, thus impeding misinterpretation (b).

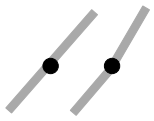

Figure 12: Line perception

Hence, as long as there is neither vertex-clutter nor edge-clutter and as long as no pair of edges incident to a common vertex forms a 180°-angle, we can expect to be able to unambiguously tell whether an edge is incident to a vertex or not. In order to attack vertex-edge clutter we therefore propose the following optimization problem. For a pair of edges incident to a common vertex p we define the *angular straight-line deviation* as the smaller of the two angles that is enclosed by the lines defined by the two edges, respectively. The angular straight-line deviation of p is then defined as the minimum angular straight-line deviation over all pairs of edges incident to p, as illustrated in Figure 13. The angular straight-line deviation of a geometric graph G is the minimum angular straight-line deviation over all vertices of G. Note that the angular straight-line deviation is maximized if all angles between edges incident to a common vertex are close to a right angle. Although it sounds similar, the concept of angular straight-line deviation differs strongly from the angular resolution. For example $K_{1,4}$, the star with four leaves, admits a drawing with optimal angular resolution $\pi/4$ by setting all angles at the center to $\pi/2$. However, the angular straight-line deviation of such a drawing is 0. The optimal angular straight-line deviation of $K_{1,4}$ is $\pi/4$, which can be achieved by having at the center three angles of $\pi/4$ and one angle of $5/4\pi$.

Given a geometric graph $G = (P, E)$ and a non-negative value $r \in \mathbb{R}^+$, the Optimal Angle Adjustment problem is to find a new position for each vertex p inside $B(p, r)$ minimizing the angular straight-line deviation of the resulting geometric graph.

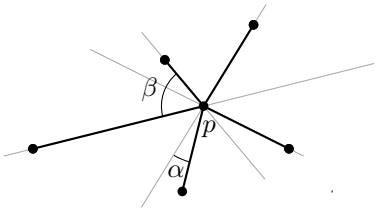

Figure 13: Angular straight-line deviation of a vertex p. In the drawing the angular straight-line deviation is defined by the angle α. Note the difference between α, which defines the angular straight-line deviation and the angle β, which defines the angular resolution at p.

Problem Optimal Angle Adjustment

Instance: Geometric graph $G = (P, E)$, $r \in \mathbb{R}_0^+$

Solution: Geometric graph $H = (Q, F)$ and a mapping $f : P \to Q$ such that $d(p, f(p)) \leq r$ and such that $f(p)f(q) \in F$ if and only if $pq \in E$

Goal: maximize the angular straight-line deviation of H

Note that this problem differs considerably from the problem of maximizing the angular resolution of a graph, defined as the minimum angle over all pairs of adjacent edges. The optimal angular resolution of a star-shaped graph with an odd number of vertices, for instance, will result in zero straight-line deviation, while it is obvious that the optimal straight-line deviation is positive. We tackle the Optimal Angle Adjustment problem by maximizing the vertices' distances from the lines defined by the edges incident to their neighbors. Let $G = (P, E)$ be a geometric graph and let $v \in P$ be a vertex. Let $N(v)$ denote its neighbors in G. Further, let $E(v)$ denote the edges incident to v and let $F(v)$ denote the set of edges incident to the vertices in $N(v)$ but not to v. By moving v we change the angles formed by pairs of edges in $E(v)$ as well as the angles formed by pairs of edges (e, f) such that $e \in E(v)$ and $f \in F(v)$, respectively. Let $L_F(v)$ be the set of lines defined by the edges in $F(v)$ and let $L_E(v)$ be the set of lines defined by all pairs of vertices in $N(v)$. A vertex v along with the lines defined by the edges in $L_E(v)$ and $L_F(v)$ is illustrated in Figure 14a. Note, that there will be an angle of 180 degrees involving an edge incident to v if and only if v is placed on one of the lines in $L_E(v) \cup L_F(v)$. Given $p \in \mathbb{R}^2$, we denote by $\mu_v(p)$ the minimum distance of p to the lines in $L_E(v) \cup L_F(v)$. We prove the following.

Theorem 5 *Given a graph $G = (P, E)$ of maximum degree Δ, a vertex $v \in P$ and a positive radius $r \in \mathbb{R}^+$, we can compute a new position p^* for v in $B(v, r)$ such that $\mu_v(p^*) > 0$ and such that p^* maximizes $\mu_v(p)$ over all $p \in B(v, r)$ in $O(t^2)$ time, where $t = \min\{\Delta^2, |E|\}$.*

Proof: First, we compute the set of edges $L_F(v)$ incident to v's neighbors, but not to v as well as the set of lines $L_E(v)$ defined by all pairs of v's neighbors.

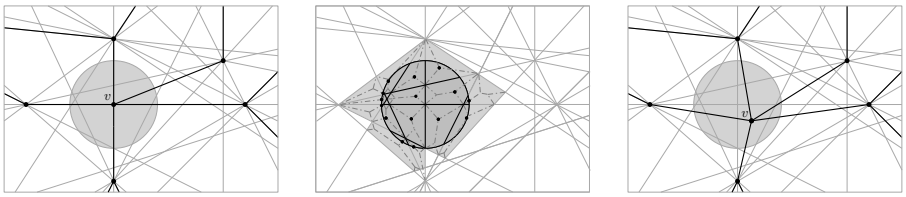

(a) (b) (c)

Figure 14: Illustration for the proof of Theorem 5. (a) A vertex v and its neighbors as well as the arrangement of lines induced by the respective edges in $L_E(v)$ and $L_F(v)$. (b) Intersection of the circle with the medial axis $\mathcal{G}_c$ (dashed) and locally optimal positions (black dots) in the faces. (c) Globally optimal position and resulting new drawing.

Let $L = L_E(v) \cup L_F(v)$. We compute the arrangement of lines in L in $O(|L|^2)$ time. Note that the optimal point $p^\star$ must lie in the interior of a face of this arrangement. Moreover, it must have the same distance from at least two segments incident to that face, otherwise a better position could be found. This is, however, precisely the definition of the medial axis of a simple polygon. Thus, the optimal point $p^\star$ lies on the medial axis of a face of the arrangement. Note that the total complexity of the arrangement is $O(|L|^2)$. We now compute for each face the medial axis. Using the linear-time algorithm due to Chin et al. [12] this takes time $O(|L|^2)$ for all faces. For each face C we inspect the vertices of the medial axis $\mathcal{G}_C$ in $B(v, r)$ as well as its intersection with $B(v, c)$ and thus compute the point p^* maximizing μ_v in $B(v, r)$. Then we update the position of v as illustrated in Figure 14c. Since L is bounded by $\min\{\Delta^2, |E|\}$ we obtain the claimed time complexity. Further, since $r > 0$ and therefore $B(v, r)$ is non-degenerate, there must be a non-degenerate face in the arrangement containing a point p^* in its interior such that $\mu(p^*) > 0$. □

Using Theorem 5 we can incrementally compute a new position for each vertex v such that none of the edges incident to v encloses an angle of 180 degrees with any other edge. Since the angles between pairs of edges that are not incident to v are not affected by this operation, we can iteratively apply Theorem 5 to the vertices one after another to obtain a drawing with strictly positive angular straight-line deviation. At the same time this approach heuristically maximizes this deviation.

Note that we may assume that we apply the angle adjustment to a generalized graph whose complexity tends to be significantly lower than the complexity of the original graph, i.e., both m and Δ should be considerably smaller.

5 Sample Generalizations

In order to evaluate the quality of the described heuristics and in order to obtain estimates for the running time we implemented the described Greedy Weight Heuristic and Monotone Drift Heuristic in C++ using the BOOST library [7] and the CGAL library [1]. All generalizations were computed on a standard Intel Core 2 Duo processor running at 2.00 GHz with 2 GB RAM.

We performed our experiments on the benchmark set of graphs listed in Table 1. These graphs have between 1,000 and 100,000 vertices and between 3,000 and 2,000,000 edges, respectively. The table lists, for each graph, an index that is used to identify the graphs in the following figures as well as its size. All but the graphs marked with $\star$ have been taken from the University of Florida sparse matrix collection [14]. The graph `clique-planar` is a planar graph with an implanted clique. The graph `lunar-vis` is a LunarVis layout [24] of a snapshot of the Internet graph at the autonomous systems level that has been taken from the data collected by the University of Oregon Routeviews Project [2]. The graph `email` is a force-based visualization of the graph obtained from the e-mail communication at the faculty of informatics at the Karlsruhe Institute of Technology during a fixed amount of time. The graphs `osm_berlin` and `osm_isleofman` are street networks of Berlin, Germany, and Isle of Man, respectively, that have been extracted from OpenStreetMap data [36]. The graphs from the University of Florida sparse matrix collection have additionally been laid out using the `sfdp` multi-scale force-based layout algorithm from the graphviz library [18].

For each of the graphs listed in Table 1 as well as for both $\alpha = 0$ and $\alpha = 1$, we performed generalizations with $N = 10$ different radii taken from the range $[\Delta/n, \Delta/\sqrt{n}]$, where $\Delta := x_{\max} - x_{\min}$ is the width of the drawing. More precisely, the ith radius r_i is chosen according to a convex combination $r_i = (1 - \lambda_i) \cdot \Delta/n + \lambda_i \cdot \Delta/\sqrt{n}$, where $\lambda_i = i/N$ for $i = 1, \ldots, N$. For each run, we measured the time t_1 of the Greedy Weight Heuristic and the time t_2 of the Monotone Drift Heuristic. Further, we collected the number of vertices n_H and the number of edges m_H of the resulting generalized graphs.

Table 1: Benchmark set of graphs used for our experiments, sorted according to number of vertices. All graphs, except those marked with $\star$, are from the University of Florida sparse matrix collection [14]; `clique-planar` is a planar graph with an implanted clique, `lunar-vis` is a LunarVis layout of the AS-Graph [24], `email` is a force-based layout of the email network of the faculty of informatics and `osm_berlin` and `osm_isleofman` are street networks extracted from the OpenStreetMap data [36].

i	name	n	m
1	bcspwr09	1036	3736
2	bcsstk08	1050	29156
3	bcsstk14	1072	12444
4	bcsstk26	1074	12960
5	can_1072	1133	10902
6	clique-planar*	1141	7465
7	bcsstk35	1242	10426
8	bcsstk36	1723	6511
9	bcsstk37	1733	22189
10	bodyy4	1806	63454
11	c-48	1821	52685
12	cti	1866	7076
13	ex3sta1	1919	32399
14	ford1	1922	30336
15	g7jac060sc	1960	11187
16	jan99jac060	1961	5156
17	jan99jac100sc	2363	7680
18	tandem_vtx	2423	11672
19	TF16	3345	19404
20	dwt_1242	6290	16466
21	email*	7920	31680

i	name	n	m
22	ex33	16558	149658
23	ex3	16782	678998
24	jagmesh8	16840	96464
25	aug3d	17233	74436
26	cep1	17546	121938
27	commanche_dual	18354	166080
28	conf5_4-8x8-05	18454	253350
29	lpl3	18728	101576
30	nemscem	23052	1143140
31	pds10	24300	69984
32	sstmodel	24494	51256
33	msc01050	25503	1140977
34	netz4504	30237	1450163
35	lunar-vis*	34758	432346
36	osm_berlin*	35460	406632
37	osm_isleofman*	41228	254364
38	plat1919	44514	201050
39	rajat02	49152	2064384
40	stufe	68908	431724
41	ukerbe1_dual	106675	248390

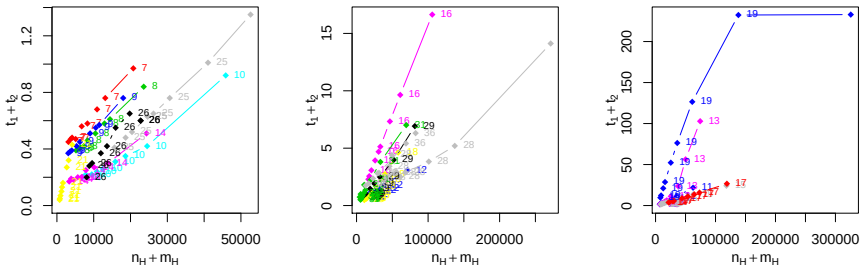

(a) $0.3 \leq t_1 + t_2 < 3$ (b) $3 \leq t_1 + t_2 < 20$ (c) $t_1 + t_2 \geq 20$

Figure 15: Running times of the generalization heuristic with respect to the size of the generalization. The plots are for $\alpha = 1$ and drift $= 0.3$. For clarity, the plot has been divided into three figures, according to the total running time $t_1 + t_2$ of the two steps of the generalization heuristic. Each curve corresponds to one of the input graphs.

Even for the largest input graphs with several thousand vertices and over a million edges, the observed running times were less than 5 minutes. However, most of the running time is caused by the Monotone Drift Heuristic, which has a quadratic worst-case running time. For the Greedy Weight Heuristic, the observed running time was less than 5 seconds for all graphs. Figure 15 shows the running time of the heuristics as a function of the size $n_H + m_H$ of the generalized graphs. Our experiments showed that the running time of the heuristic depends quite strongly on the size of the generalized graph it produces. Since, in practice, we expect that generalizations will be quite small compared to the input graphs, this suggests that for practical purposes, an output-sensitive analysis, which relates the output size to the running time, is more appropriate than an evaluation based on the input size. In the following, we back up this claim with experimental data and use it to estimate a polynomial that describes the running time depending on the output size.

Figure 15 shows the running time of the heuristics as a function of the size $n_H + m_H$ of the generalized graphs. Figures 15a–15c display the running times for $\alpha = 1$ for the individual graphs of our benchmark on a linear scale. The results for $\alpha = 0$ are similar. Figure 15a contains all graphs for which $t_1 + t_2$ was at most 3 seconds, Figure 15b contains all graphs whose maximum running time was between 3 and 20 seconds and Figure 15c contains all graphs whose running time was more than 20 seconds. The strong dependence of output size and running time is quite notable in these sets. Note that, if we would relate the running times to the input size rather than the output size, each of the curves in these plots would have to be represented by a single dot, which obviously would not properly describe the running times. In fact, with only a few exceptions, such as `ex3sta1`, `TF16` and `conf5_4-8x8-05`, the running times seem to roughly linear in the size of the generalized graph. Thus, with respect to the output size,

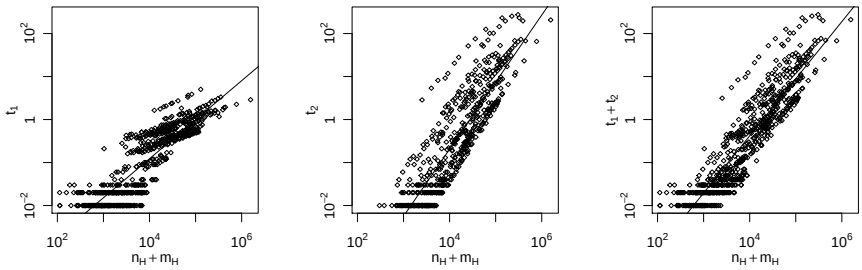

(a) Vertex Clutter (b) Edge Clutter (c) Total

Figure 16: Breakdown of the running time of the generalization heuristic to vertex clutter, edge clutter and total time, respectively, in a log-scale plot. The slope of the line fitted to these points is an estimate for the exponent of a polynomial that relates the size of the generalization to the running time.

we can expect that the running time can indeed be described by a polynomial of low degree, which would imply good practical performance.

Figure 16 shows the running times of the two heuristics Greedy Weight Heuristic and Monotone Drift Heuristic both separately and in total. To fit all data into one plot we use a log-log-scale plot for these figures. Figure 16a shows the running time t_1 of the Greedy Weight Heuristic, Figure 16b shows the running time t_2 of the Monotone Drift Heuristic and Figure 16c shows the resulting combined running time. To estimate a polynomial dependency between input and output size, we fit a line to each of these plots. The slope of this line is the largest exponent of the polynomial expressing the dependency. More precisely, for $x = n_H + m_H$ and for each $y \in \{t_1, t_2, t_1 + t_2\}$, we computed a_y and b_y minimizing the linear least-squares function

$$\min_{a_y, b_y \in \mathbb{R}} \sum_{i=1}^{N} (\log y_i - (a_y \log x_i + b_y))^2$$

where x_i and y_i denote the measured sizes and running times of the single experiments for $i = 1, \ldots, N$, respectively. The estimated lines are shown in the plots in Figure 16. The results suggest that the running time of the Greedy Weight Heuristic $t_1 \approx e^{-10.4578} x^{0.9076}$ is approximated by a function that is slightly sub-linear in the size of the generalized graph and the running time of the Monotone Drift Heuristic $t_2 \approx e^{-15.95} x^{1.56}$ is approximated by a super-linear but sub-quadratic function in the size of the generalized graph. The combined running time is approximately $t_1 + t_2 \approx e^{-13.105} x^{1.328}$, which is super-linear, but only slightly. We can thus expect that in practice the running time is subquadratic in the output size, which is reasonable for generalized graphs of moderate size. Note that the running time of the first phase depends only on the number of vertices, whereas the output size includes both the number of vertices and the number of edges in the resulting generalization. Since most of

the graphs in our test set have more than linearly many edges, sublinear running times can be achieved in the first phase.

Next, we shortly discuss the generalized graphs. Figure 17 shows how the parameter α affects the generalization. While the sizes of the generalized graphs for $\alpha = 0$ and $\alpha = 1$ will, in general, differ considerably for a fixed radius r, we chose generalized graphs with roughly the same sizes in order to illustrate the effects of choosing $\alpha = 0$ and $\alpha = 1$, respectively. Figure 17 clearly shows that the generalizations with $\alpha = 1$ are better suited at preserving the distribution of the original point set also in denser areas. However, this is only achieved at the price of a higher resolution of the resulting drawing. On the other hand, the homogeneous distribution of the points resulting from $\alpha = 0$ does not seem to capture the geometric properties of the original very well. Especially denser areas rapidly approach a uniform distribution with exactly the same fixed amount of empty space around each point. Only the density of input regions that are sparser then this are preserved by the corresponding generalizations. Indeed, it seems that setting $\alpha = 0$ is not well suited for most of the graphs we inspected due to this behavior. Therefore, all remaining generalization are performed with $\alpha = 1$ unless stated otherwise.

Figure 18 shows how the radius r and the drift δ impact the resulting generalizations for $\alpha = 1$. To illustrate the effects of δ we applied the Greedy Weight Heuristic and Monotone Drift Heuristic for different values of r and δ to a planar graph with an implanted clique whose vertices have been arranged equidistantly on a cycle. While none of the edges of the clique are distinctly perceivable in the original drawing, a higher drift helps remedying this without destroying the impression of a clique even without generalizing the vertex set, as can be seen in the first row of Figure 18. Note that the clique in the middle of the drawing remains a clique when setting $\delta = 0$ for all values of r. With increasing δ, the clique becomes much sparser but is still perceivable as a rather dense subgraph in the generalized graph for all radii.

Finally, Figures 19–26 show some selected sample generalizations. First, we discuss how the heuristics perform on the graphs we used to illustrate the various types of clutter in Figure 1c. These graphs as well as the results of the heuristic generalization are displayed in Figures 19–21. Note that the displayed generalized graphs have only 2–5% of the vertices of the respective originals. Clearly, both vertex-clutter and edge-clutter can be significantly reduced without changing the main impression of the graph. However, two drawbacks of our approach are immediately obvious from these illustrations.

First, consider the graph `oix` and its generalization in Figures 20a and 20b, respectively. In the original, there are many edges between a few vertices on the left and the vertices in the bottom center. Apparently, these edges are mapped to only few monotone paths in the generalization, which changes the impression of the density of the edges. This could be tackled by emphasizing the edges in the generalization according to the number of edges that were mapped to it. As another approach to this problem, we could try to approximate the geometric edge distribution. That is, similar to our approximation of the point-set distribution, we could try to remove more edges from regions containing

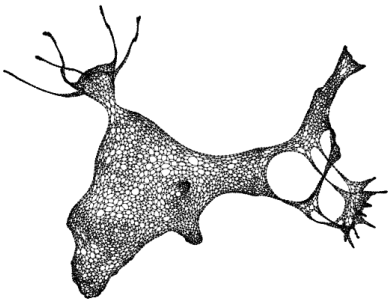

(a) original (n=7920, m=31680)

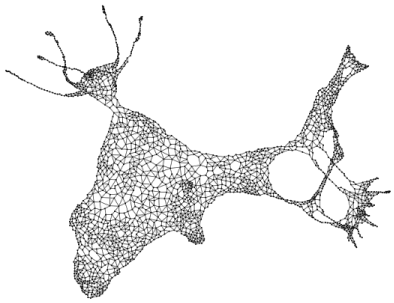

(b) generalization (n=2104, m=8585)

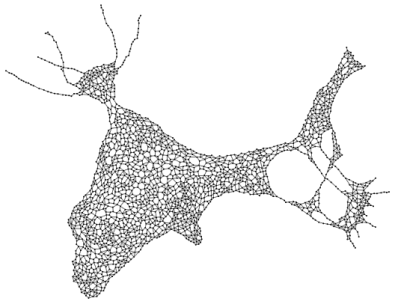

(d) generalization (n=2098, m=8188)

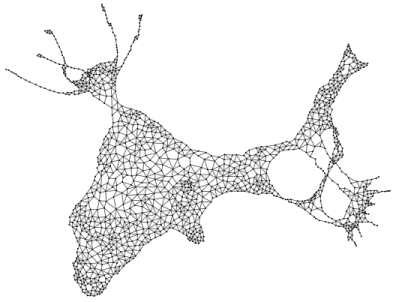

(c) generalization (n=1305, m=5636)

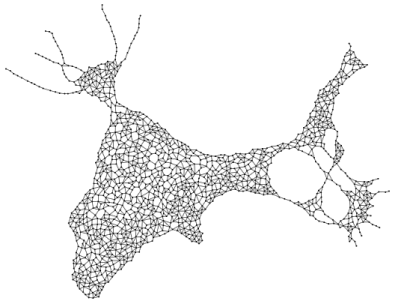

(e) generalization (n=1358, m=5678)

Figure 17: Effects of parameter α on the `commanche_dual` graph from the University of Florida sparse matrix collection [14]. (a) Original, (b), (c) Generalization with $\alpha = 1$, (d), (e) Generalization with $\alpha = 0$.

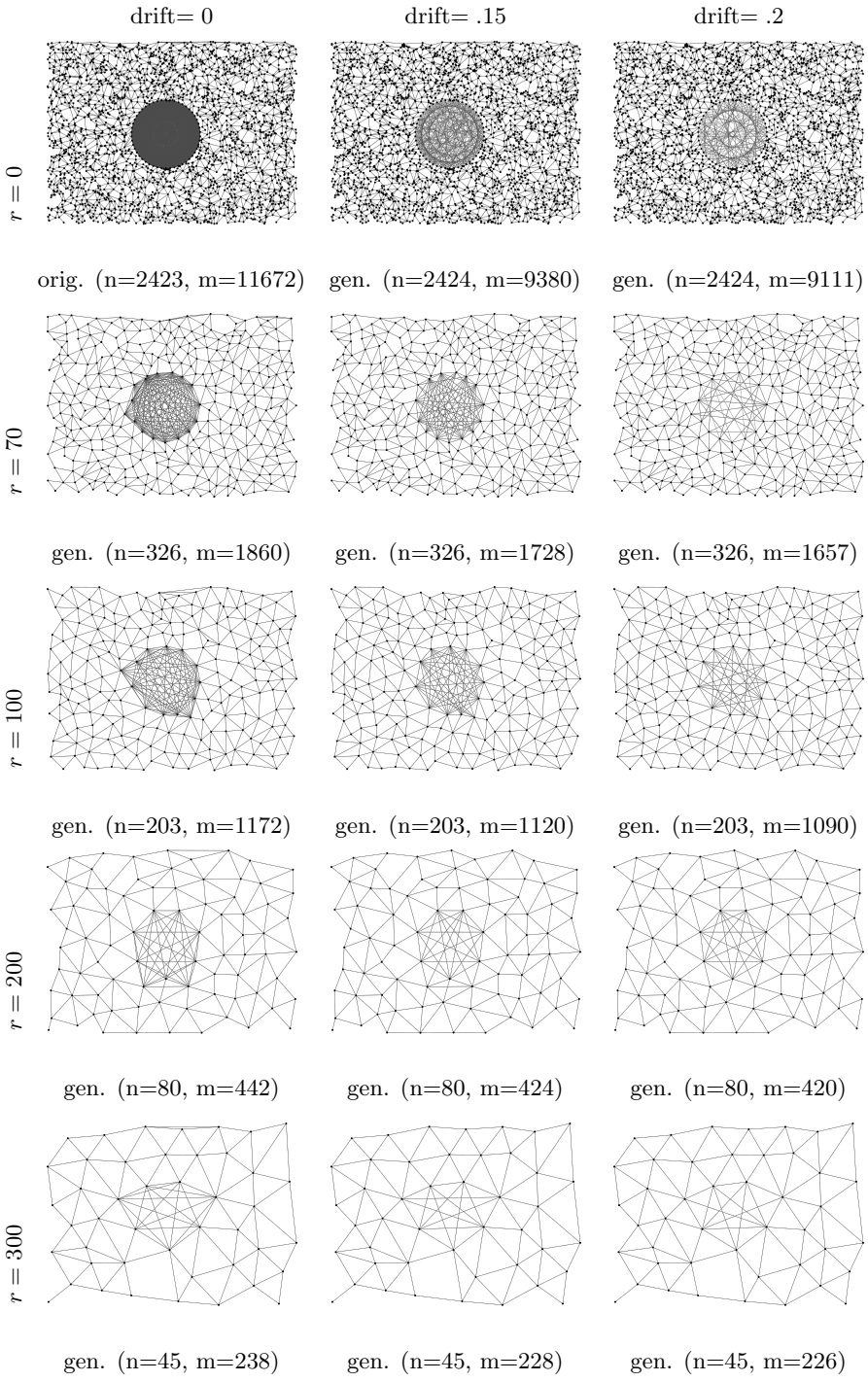

Figure 18: Effect of radius and drift on the graph `clique-planar`, a planar graph with an implanted clique. All generalizations with $\alpha = 1$.

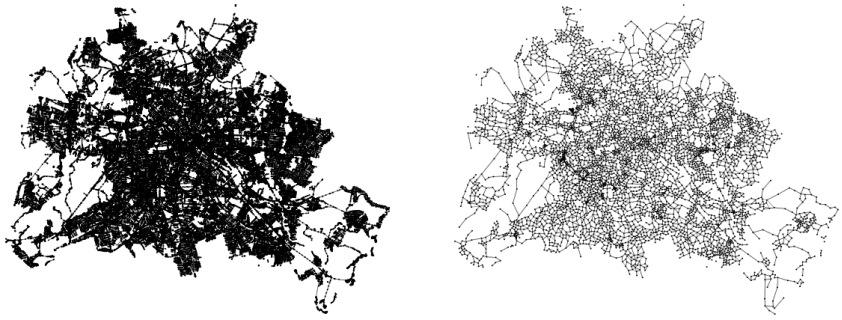

(a) original (n=106675, m=248390) (b) generalization (n=5649, m=17273)

Figure 19: Streetmap Data of Berlin [36] (`osm_berlin`)

few edges and removing fewer edges in regions with many edges. In contrast to approximating the point-set distribution, however, it is not clear how to achieve this in a straightforward way since a single edge may cross both dense and less dense regions in the drawing.

Second, consider the graph `PDS10` and its generalization in Figures 21a and 21b, respectively. Clearly, the topmost vertices of the generalization show that our approach may create unwanted adjacencies. These adjacencies are the result of contracting vertices that are close to each other and working on the contracted edge set. While the edges are not false in the sense that each edge in the contraction corresponds to at least one edge of the original, these edges create the wrong visual impression. This problem could be approached by trying to approximate the features of the contracted vertex sets. For instance, the average degree of the contracted vertex sets will be roughly two for most of the problematic vertices in these figures, while the resulting degree in the generalization is larger.

The remaining figures serve as a further visual benchmark of the generalization heuristics. While the general (geometric) impression of the graphs are reasonably well maintained, some further issues for future research can be observed.

Consider for example the graph `ukerbe1_dual` and its generalization illustrated in Figure 24a and 24b, respectively. While the density of the point set and the size of the faces is maintained quite well, most of the faces are triangulated in the generalization, whereas most of the faces of the original contain four vertices. Further, consider the "cube graph" illustrated in Figure 25. The topological structure of the generalized graph is rather different from the original. Although the vertices contracted into single clusters are close to each other both geometrically and with respect to graph-distance, the cubic structure is

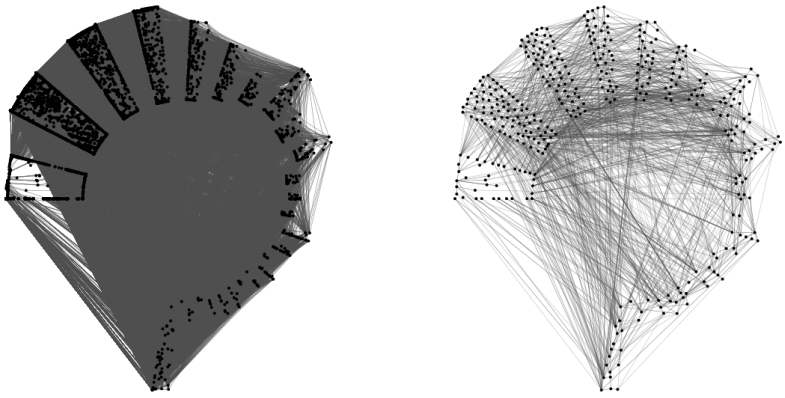

(a) original (n=17233, m=74436) (b) generalization (n=397, m=2134)

Figure 20: LunarVis Layout of the AS-Graph [24] (`lunar-vis`)

not maintained. Again this may be remedied by approximating the features of the contracted vertices, such as average degree.

While the proposed heuristics do not solve the generalization problem in all its facets, especially with respect to the topological features of the graph, they seem to be well suited at maintaining the geometric impression of the originals and, thus, form good starting points for future research on this problem. In order to overcome the current difficulties, however, we must explicitly include topological features of the original graph into the generalization process. We showcase some further examples without a detailed discussion in Figures 21–26.

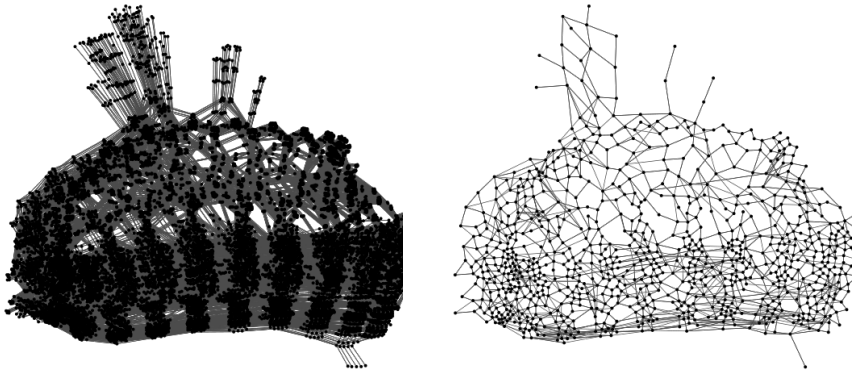

(a) original (n=16558, m=149658) (b) generalization (n=910, m=3520)

Figure 21: Generalization of the graph `PDS10` from the University of Florida sparse matrix collection [14]

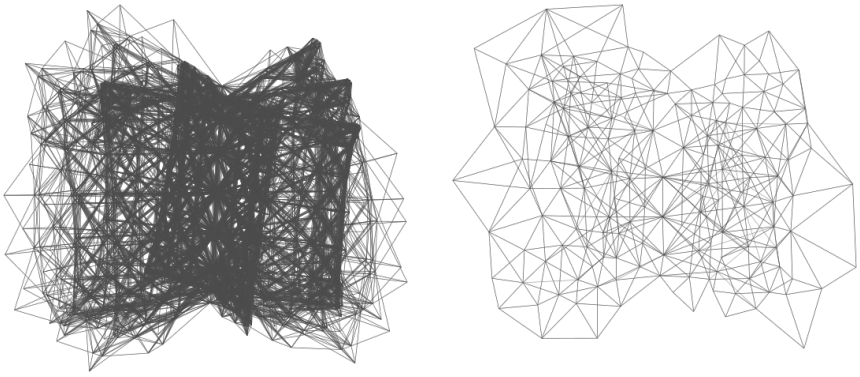

(a) original (n=1050, m=29156) (b) generalization (n=157, m=1110)

Figure 22: Generalization of the graph `msc01050` from the University of Florida sparse matrix collection [14]

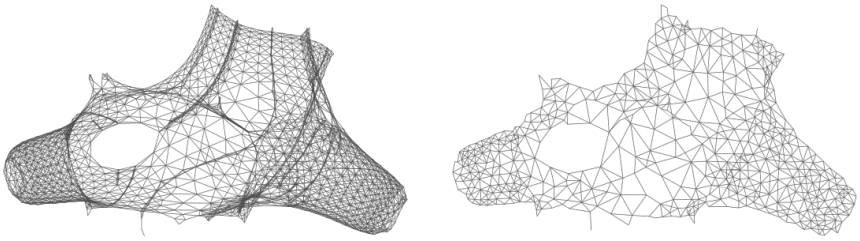

(a) original (n=1242, m=10426) (b) generalization (n=469, m=2608)

Figure 23: Generalization of the graph `dwt_1242` from the University of Florida sparse matrix collection [14]

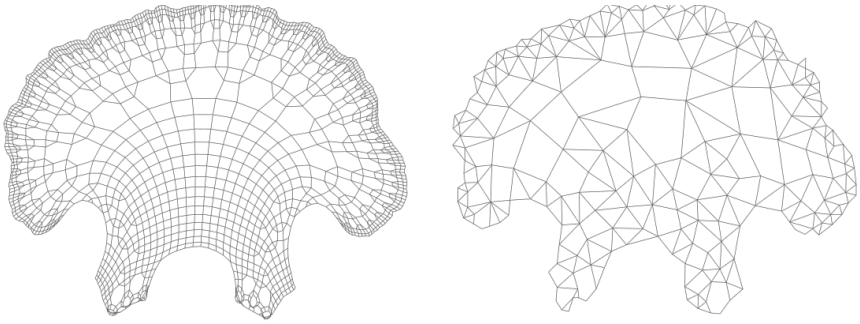

(a) original (n=1866, m=7076) (b) generalization (n=234, m=1062)

Figure 24: Generalization of the graph `ukerbe1_dual` from the University of Florida sparse matrix collection [14]

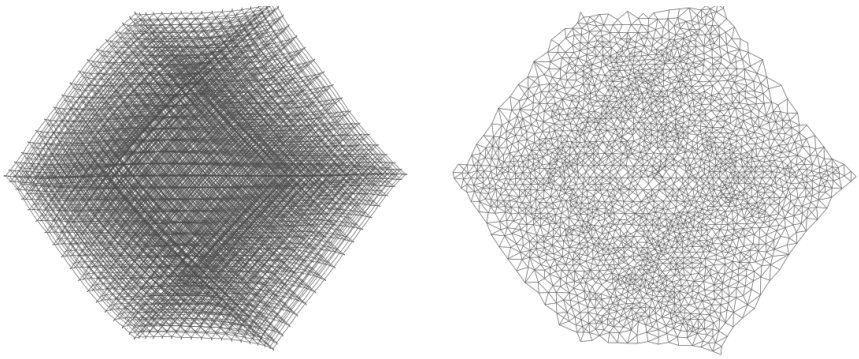

(a) original (n=24300, m=69984) (b) generalization (n=2093, m=13546)

Figure 25: Generalization of the graph `aug3d` from the University of Florida sparse matrix collection [14]

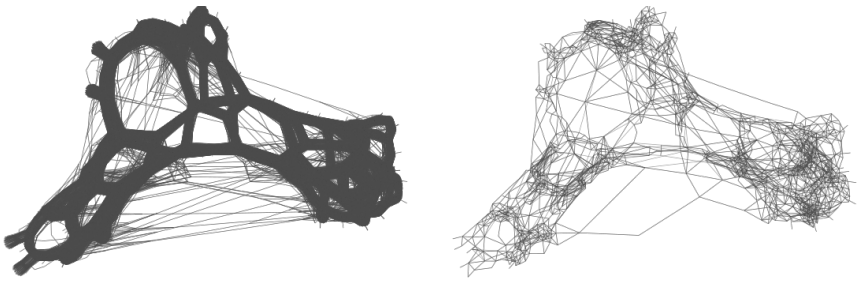

(a) original (n=44514, m=201050) (b) generalization (n=958, m=5763)

Figure 26: Generalization of the graph `lpl3` from the University of Florida sparse matrix collection [14]

6 Conclusion and Open Problems

We have undertaken a first step at studying the problem of generalizing geometric graphs within a rigorous mathematical model. We formalized the problem by considering an incremental framework modeling the elimination or reduction of different types of clutter as optimization problems, which we analyzed in terms of complexity. Since these problems turned out to be NP-hard in general, we also devised efficient approximation algorithms as well as efficient heuristics. We showed how to heuristically reduce vertex-clutter in $O((n+m)\log^3 m + n\log^2 n)$ time and how to reduce edge clutter in $O(nm+m^2)$ time, considering geometric features such as point distributions and geodesic tendencies. After the reduction of vertex-clutter and edge-clutter, we can expect the graph to be much smaller than the original graph. Hence, even larger complexities may scale accordingly. Thus, even the relatively high complexity of our heuristic for reducing vertex-edge clutter may be practical.

Even without this step, however, the resulting generalizations exhibit considerably less clutter and are easier to analyze. We showcased some promising generalizations produced by our heuristics. We conclude by listing some open problems.

- Is it possible to approximate both the local coverage and the size of a ϱ-set in the vertex generalization step?
- What is the complexity of the Local Coverage Cluster Packing problem for different types of mappings?
- Is it possible to approximate the size of a shortest geodesic subgraph, possibly in the presence of a limited drift?
- What is the complexity of the optimal angle adjustment problem?
- How can the generalization problem be adapted to a dynamic scenario, where consistency issues play an additional role.

In addition, a major open problem is to define a measure that can be used to quantitatively compare different generalizations of a graph. Such a measure would need to quantify both the graph-theoretic similarities between a graph and its generalization and the similarity of the corresponding visualization. Finding such a measure would also make it possible to perform a more extensive experimental evaluation of the proposed methods and the quality resulting from different parameter choices.

Acknowledgements

We thank Robert Görke for the helpful discussion and for providing the LunarVis layout. We also thank thank the anonymous referees of the journal version of this paper for their valuable comments, which helped us to improve both the results and the presentation.

References

[1] CGAL, Computational Geometry Algorithms Library. http://www.cgal.org.

[2] University of oregon routeviews project. http://www.routeviews.org/.

[3] J. Abello, S. Kobourov, and R. Yusufov. Visualizing large graphs with compound-fisheye views and treemaps. In J. Pach, editor, *Proceedings of the 12th International Symposium on Graph Drawing (GD'04)*, volume 3383 of *Lecture Notes in Computer Science*, pages 431–441. Springer, 2005. doi:10.1007/978-3-540-31843-9_44.

[4] J. Abello, J. Korn, and I. Finocchi. Graph sketches. In *Proceedings of the IEEE Symposium on Information Visualization 2001 (INFOVIS'01)*, pages 67–70. IEEE Computer Society, 2001. doi:10.1109/INFVIS.2001.963282.

[5] J. L. Bentley and J. B. Saxe. Decomposable searching problems I. static-to-dynamic transformation. *Journal of Algorithms*, 1(4):301–358, 1980. doi:10.1016/0196-6774(80)90015-2.

[6] R. E. Bohn and J. E. Short. How much information? 2009 Report on American consumers. Global Information Industry Center, University of California, San Diego, 2009. URL: http://hmi.ucsd.edu/howmuchinfo_research_report_consum.php.

[7] Boost C++ libraries, version 1.42. http://www.boost.org.

[8] P. Bose, V. Dujmović, F. Hurtado, J. Iacono, S. Langerman, H. Meijer, V. Sacristán, and M. Saumell. Proximity graphs: E, δ, Δ, χ and ω. *International Journal of Computational Geometry and Applications*, 22(5):439–470, 2012. doi:10.1142/S0218195912500112.

[9] U. Brandes, D. Delling, M. Gaertler, R. Görke, M. Hoefer, Z. Nikoloski, and D. Wagner. On modularity clustering. *IEEE Trans. Knowledge and Data Engineering*, 20:172–188, 2008. doi:10.1109/TKDE.2007.190689.

[10] P. Callahan and S. Kosaraju. A decomposition of multidimensional point sets with applications to k-nearest-neighbors and n-body potential fields. *Journal of the ACM*, 42(1):67–90, 1995. doi:10.1145/129712.129766.

[11] B. Chazelle. Functional approach to data structures and its use in multidimensional searching. *SIAM J. Comput.*, 17:427–462, 1988. doi:10.1137/0217026.

[12] F. Chin, J. Snoeyink, and C. Wang. Finding the medial axis of a simple polygon in linear time. In *Proceedings of the 6th International Symposium on Algorithms and Complexity (ISAAC'95)*, pages 382–391, 1995. doi:10.1007/PL00009429.

[13] B. N. Clark, C. J. Colbourn, and D. S. Johnson. Unit disk graphs. *Discrete Mathematics*, 86(1-3):165 – 177, 1990. doi:10.1016/0012-365X(90)90358-O.

[14] T. A. Davis. University of florida sparse matrix collection. *NA Digest*, 92, 1994.

[15] M. de Berg and A. Khosravi. Optimal binary space partitions for segments in the plane. *International Journal of Computational Geometry & Applications*, 22(3):187–205, 2012. doi:10.1142/S0218195912500045.

[16] D. Dobkin, S. Friedman, and K. Supowit. Delaunay graphs are almost as good as complete graphs. *Discrete & Computational Geometry*, 5:399–407, 1990. doi:10.1007/BF02187801.

[17] P. Eades and Q.-W. Feng. Multilevel visualization of clustered graphs. In S. North, editor, *Graph Drawing*, volume 1190 of *Lecture Notes in Computer Science*, pages 101–112. Springer, 1997. doi:10.1007/3-540-62495-3_41.

[18] J. Ellson, E. Gansner, E. Koutsofios, S. North, and G. Woodhull. Graphviz and dynagraph – static and dynamic graph drawing tools. In M. Junger and P. Mutzel, editors, *Graph Drawing Software*, pages 127–148. Springer, 2003. doi:10.1007/978-3-642-18638-7_6.

[19] G. W. Furnas. Generalized fisheye views. *SIGCHI Bull.*, 17:16–23, April 1986. doi:10.1145/22339.22342.

[20] M. Gaertler. Clustering. In U. Brandes and T. Erlebach, editors, *Network Analysis*, volume 3418 of *Lecture Notes in Computer Science*, pages 178–215. Springer, 2005. doi:10.1007/978-3-540-31955-9_8.

[21] P. Gajer and S. Kobourov. Grip: Graph drawing with intelligent placement. *Journal of Graph Algorithms and Applications*, 6(3):203–224, 2002. doi:10.7155/jgaa.00052.

[22] E. Gansner, Y. Koren, and S. North. Topological fisheye views for visualizing large graphs. *Visualization and Computer Graphics, IEEE Transactions on*, 11(4):457–468, 2005. doi:10.1109/TVCG.2005.66.

[23] M. R. Garey and D. S. Johnson. *Computers and Intractability. A Guide to the Theory of NP-Completeness*. W. H. Freeman and Company, 1979.

[24] R. Görke, M. Gaertler, and D. Wagner. Lunarvis - analytic visualizations of large graphs. In S.-H. Hong, T. Nishizeki, and W. Quan, editors, *Proceedings of the 15th international conference on Graph drawing (GD'07)*, volume 4875 of *Lecture Notes in Computer Science*, pages 352–364. Springer, 2008. doi:10.1007/978-3-540-77537-9_35.

[25] S. Hachul and M. Jünger. Drawing large graphs with a potential-field-based multilevel algorithm. In J. Pach, editor, *Proceedings of the 12th International Symposium on Graph Drawing (GD'04)*, volume 3383 of *Lecture Notes in Computer Science*, pages 285–295. Springer, 2005. doi:10.1007/978-3-540-31843-9_29.

[26] M. Halldórsson and J. Radhakrishnan. Greed is good: Approximating independent sets in sparse and bounded-degree graphs. *Algorithmica*, 18:145–163, 1997. doi:10.1007/BF02523693.

[27] D. Harel and Y. Koren. A fast multi-scale method for drawing large graphs. *Journal of Graph Algorithms and Applications*, 6(3):179–202, 2002. doi:10.7155/jgaa.00051.

[28] D. Harel and Y. Koren. Graph drawing by high-dimensional embedding. *Journal of Graph Algorithms and Applications*, 8(2):195–214, 2004. doi:10.7155/jgaa.00089.

[29] D. Holten and J. J. van Wijk. Force-directed edge bundling for graph visualization. *Computer Graphics Forum*, 28(3):983–990, 2009. doi:10.1111/j.1467-8659.2009.01450.x.

[30] W. Huang, P. Eades, and S.-H. Hong. A graph reading behavior: Geodesic-path tendency. In *Proceedings of the IEEE Pacific Visualization Symposium (PacificVis'09)*, pages 137–144, 2009. doi:10.1109/PACIFICVIS.2009.4906848.

[31] Y. Koren, L. Carmel, and D. Harel. Drawing huge graphs by algebraic multigrid optimization. *Multiscale Modeling and Simulation*, 1:645–673, 2003. doi:10.1137/S154034590241370X.

[32] M. Li and P. M. Vitnyi. *An Introduction to Kolmogorov Complexity and Its Applications*. Springer, 3 edition, 2008.

[33] W. A. Mackaness and K. M. Beard. Use of graph theory to support map generalization. *Cartography and Geographic Information Science*, 20:210–221, 1993.

[34] W. A. Mackaness, A. Ruas, and L. T. Sarjakoski, editors. *Generalisation of Geographic Information*. Cartographic Modelling and Applications. Elsevier B.V., 2007.

[35] K. Misue, P. Eades, W. Lai, and K. Sugiyama. Layout adjustment and the mental map. *Journal of Visual Languages & Computing*, 6(2):183–210, 1995. doi:10.1006/jvlc.1995.1010.

[36] Openstreetmap database. online, 2011. http://www.openstreetmap.de/.

[37] A. Quigley and P. Eades. FADE: Graph drawing, clustering, and visual abstraction. In J. Marks, editor, *Proceedings of the 8th International Symposium on Graph Drawing (GD'00)*, volume 1984 of *Lecture Notes in Computer Science*, pages 77–80. Springer, 2001. doi:10.1007/3-540-44541-2_19.

[38] D. Rafiei and S. Curial. Effectively visualizing large networks through sampling. In *Visualization, 2005. VIS 05. IEEE*, pages 375–382, 2005. doi:10.1109/VISUAL.2005.1532819.

[39] A. Saalfeld. Map generalization as a graph drawing problem. In R. Tamassia and I. Tollis, editors, *Graph Drawing*, volume 894 of *Lecture Notes in Computer Science*, pages 444–451. Springer, 1995. doi:10.1007/3-540-58950-3_398.

[40] M. Sarkar and M. H. Brown. Graphical fisheye views of graphs. In *Proceedings of the SIGCHI Conference on Human Factors in Computing Systems*, CHI '92, pages 83–91. ACM, 1992. doi:10.1145/142750.142763.

[41] A. Telea and O. Ersoy. Image-based edge bundles: Simplified visualization of large graphs. *Computer Graphics Forum*, 29(3):843–852, 2010. doi:10.1111/j.1467-8659.2009.01680.x.

[42] C. Walshaw. A multilevel algorithm for force-directed graph-drawing. *Journal of Graph Algorithms and Applications*, 7(3):253–285, 2003. doi:10.7155/jgaa.00070.